Disordered flat phase and phase diagram for restricted solid-on-solid models of fcc (110) surfaces

Giuseppe Santoro, Michele Vendruscolo, and Santi Prestipino
Istituto Nazionale per la Fisica della Materia (I.N.F.M.) and International School for Advanced Studies (S.I.S.S.A.), Via Beirut 4, 34014 Trieste, Italy

Erio Tosatti
Istituto Nazionale per la Fisica della Materia (I.N.F.M.) and International School for Advanced Studies (S.I.S.S.A.), Via Beirut 4, 34014 Trieste, Italy
and International Centre for Theoretical Physics (I.C.T.P.), Trieste, Italy
(Received 18 December 1995)

We discuss the results of a study of restricted solid-on-solid model Hamiltonians for fcc (110) surfaces. These models are simple modifications of the exactly solvable body-centered solid-on-solid model, and are able to describe a (2×1) missing-row reconstructed surface as well as an unreconstructed surface. They are studied in two different ways. The first is by mapping the problem onto a quantum spin-$\frac{1}{2}$ one-dimensional Hamiltonian of the Heisenberg type, with competing $S_i^z S_j^z$ couplings. The second is by standard two-dimensional Monte Carlo simulations. We find phase diagrams with the following features, which we believe to be quite generic: (i) two flat, ordered phases (unreconstructed and missing-row reconstructed); a rough, disordered phase; an intermediate disordered flat phase, characterized by monoatomic steps, whose physics is shown to be akin to that of a dimer spin state. (ii) A transition line from the (2×1) reconstructed phase to the disordered flat phase showing exponents that appear to be close, within our numerical accuracy, to the two-dimensional Ising universality class. (iii) A critical (preroughening) line with variable exponents, separating the unreconstructed phase from the disordered flat phase. Possible signatures and order parameters of the disordered flat phase are investigated. [S0163-1829(96)04620-0]

I. INTRODUCTION

Surfaces of fcc metals, in particular (110) faces, display a variety of phase transitions, which have been the subject of considerable experimental and theoretical work. Experimentally, the (110) faces of some fcc metals — such as Au or Pt — reconstruct at low temperature into a (2×1) missing-row (MR) or related structures, whereas other metals — such as Ag, Ni, Cu, Rh, and Pd — retain (at least when clean) their bulklike periodicity. As temperature is raised, reconstructed surfaces tend to show two separate transitions: a critical deconstruction transition, and, at a higher temperature, a Kosterlitz-Thouless roughening transition.[1,2] On the other hand, unreconstructed surfaces have not been shown, so far, to reveal a similar two-transition scenario. Only a roughening transition is well documented in this case.[3,4]

Based on theoretical considerations and on simulation work, an interesting and nontrivial interplay has been anticipated between in-plane disordering, related to deconstruction, and vertical disordering, related to roughening,[5] and many other studies have been devoted to the problem.[6–12] The situation is, in principle, somewhat different for the two types of situations, i.e., the unreconstructed and the MR reconstructed cases. On an fcc (110) surface one can identify two interpenetrating rectangular sublattices, with origin, say, at 0 (the ''white'' sublattice) and A at $(\sqrt{2}\hat{\mathbf{x}}+\hat{\mathbf{y}}+\hat{\mathbf{z}})a/2$ (the ''black'' sublattice) where a is the lattice parameter, $\hat{\mathbf{x}}=(001)$, $\hat{\mathbf{y}}=(1\bar{1}0)$, and $\hat{\mathbf{z}}=(110)$. The unreconstructed (ideal) surface has therefore *two* $T=0$ ground states, differing for the sublattice that occupies the top layer (see Fig. 3). den Nijs has argued that, in such a case, the phase diagram should be qualitatively the same as that of a simple cubic (100) surface.[13] In particular, den Nijs,[13] Jug and Tosatti,[14] Kohanoff, Jug, and Tosatti,[7] and Mazzeo *et al.*[11] argued that (110) surfaces such as those of Ag and Pd (which do not reconstruct) are good candidates for realizations of *preroughening*, a critical (nonuniversal) transition from a low-temperature ordered phase to an intermediate *disordered flat* phase, previously identified in the context of restricted solid-on-solid models for simple cubic (100) surfaces.[15] In terms of the two ground states of the unreconstructed surface, the preroughening transition can be viewed as a disordering of the surface due to the proliferation of monoatomic steps (see Fig. 2) separating terraces with one type of ground state from others where the other ground state is locally present. These steps retain, however, an up-down long-range-order — stabilized by a combination of up-up (down-down) step repulsion and entropy — which prevents the surface from being rough.[15]

On the (2×1) MR reconstructed surfaces, with half of the $(1\bar{1}0)$ close-packed rows missing, the periodicity in the (001) direction is doubled. The surface therefore has *four* degenerate $T=0$ ground states, which can be classified by a clock variable $\theta=0,\pi/2,\pi,3\pi/2$, according to the ''color'' and the position of the MR in the doubled unit cell, i.e., determined by which of the four sublattices sits in the top layer (see Fig. 3). The elementary extended defects that one can consider here were discussed by Vilfan and Villain[8] and den Nijs[9] (see Fig. 2). These are (a) *steps*, which simultaneously change the average height by $\Delta h=\pm1$, and the reconstruction variable θ by $\Delta\theta=\pi/2$ [*clockwise* or (3×1) steps] or $\Delta\theta=-\pi/2$ [*anticlockwise* or (1×1) steps], and (b) *Ising wall defects* with $\Delta h=0$ and $\Delta\theta=\pi$, which can be seen as a tightly bound state between two steps of opposite

sign (up and down), but the *same* $\Delta\theta$.[9]

In this framework, den Nijs introduced a phenomenological four-state clock-step model to describe the interplay between reconstruction and roughening degrees of freedom.[9] The model is formulated on a length scale larger than microscopic, through the introduction of a coarse-grained lattice of cells in which an integer variable $h_{\mathbf{r}}$, representing the average height in the cell, and a clock reconstruction variable $\theta_{\mathbf{r}}$ are defined. A bond in the lattice can be either empty (no defect), or occupied by an up or down step of either kind, or doubly occupied by an up and down step of the same kind (equivalent to an Ising wall). den Nijs found that when (1×1) and (3×1) steps have the same energy — the so-called *zero chirality limit* — the model displays two possible scenarios: (i) If the energy of an Ising wall E_w is less than roughly twice the energy of a step E_s, temperature drives the system from the ordered phase to a disordered flat phase through an Ising transition, and then to a rough phase through a Kosterlitz-Thouless (KT) transition. (ii) When steps are energetically favored, $E_w>2E_s$, the system undergoes a single roughening-plus-deconstruction transition, which is Ising-like for the reconstruction degrees of freedom and KT-like for the height degrees of freedom. The disordered flat phase present for $E_w<2E_s$ is quite clearly characterized by the proliferation of Ising wall defects (their free energy per unit length goes to zero at the deconstruction). Accordingly, the surface shows a prevalence of $\theta=0$ and $\theta=\pi$ terraces, say, over $\theta=\pi/2$ and $\theta=3\pi/2$ ones. Using the terminology introduced in Ref. 12, such a phase could be called disordered even flat (DEF). It has an obvious nonzero order parameter that counts the difference in the abundance of $\theta=0,\pi$ terraces over that of $\theta=\pi/2,3\pi/2$ ones, and vanishing only in the rough phase. By contrast, when single steps dominate — i.e., $2E_s<E_w$ — there is apparently no mechanism, in this simple model, that may stabilize the up-down long-range order for steps, typical of disordered flat phases. It has been argued that suitable interactions penalizing the crossing of two up-up or two down-down steps — not considered by den Nijs — could stabilize such a hypothetical step-dominated disordered flat phase.[12] A disordered flat phase of this kind — termed DOF in Ref. 12 — should be characterized by an equal abundance of all types of cells $\theta=0,\pi/2,\pi,3\pi/2$, i.e., by *a vanishing of the order parameter characterizing the DEF phase*.[12]

Interestingly, the situation does not change much in the so-called *strong chirality limit* considered by den Nijs, i.e., when anticlockwise steps, say, are very costly and thus completely negligible. In such a case the problem may be mapped onto a one-dimensional fermionic model containing a Hubbard-type on-site step-step interaction U such that the energy of an Ising wall configuration (doubly occupied site) is $E_w=2E_s+U$.[16] For $U<0$, the result is the same as in the zero chirality limit case, i.e., a DEF phase is obtained. When steps dominate — i.e., for $U>0$ — two distinct rough phases appear, the deconstruction transition is no longer of the Ising type, but, again, no disordered flat phase exists.

The variety of possibilities introduced by the phenomenological models is thus very rich. Do *microscopic* models display just the same, or any new features, one might ask? In the light of the previous discussion, the question naturally arises as to what kind of disordered flat phase (or phases) is realized in simple solid-on-solid (SOS) models. The question has been considered by Mazzeo *et al.*, who have introduced, and studied by Monte Carlo simulation, a restricted SOS model that is able to deal with both unreconstructed and reconstructed situations.[11] Their model — which we will refer to as ''K_3 model'' — is a simple modification of the exactly solvable body-centered solid-on-solid model[17] (BCSOS) obtained by adding a further neighbor interaction, which can stabilize the (2×1) MR reconstruction if required. For a reconstructed case, they find two transitions: a two-dimensional (2D) Ising deconstruction to a disordered flat phase, and a KT roughening at a slightly higher temperature. The unreconstructed case studied also shows two transitions, with a nonuniversal critical transition to a disordered flat phase followed by a KT roughening.[11] The nature of the disordered flat phase present in the model was, however, not fully characterized.

In the spirit of investigating simple but fully microscopic models, Santoro and Fabrizio have studied a slightly different modification of the BCSOS model, which will be referred to as the ''K_4 model.''[18] They found that this model could be mapped onto a quantum spin-1/2 Heisenberg chain with further-neighbor interactions.[19] The phase diagram they obtained has two low-temperature ordered phases — unreconstructed or (2×1) MR reconstructed, depending on the parameters of the interactions — a high-temperature rough phase, and an intermediate disordered flat phase. The physics of the disordered flat phase was argued, by analytical arguments, to be akin to that of the *dimer quantum spin phase* studied by Haldane,[20] i.e., a doubly degenerate state that breaks translational invariance and in which dimer-dimer correlation functions acquire long-range order.

In this paper we extend and apply the approach of Ref. 18 in such a way as to provide a unified picture of the phase diagram of all the simple BCSOS-like microscopic models of fcc (110) surfaces studied so far. First we show that a quantum spin-$\frac{1}{2}$ Hamiltonian also underlies the more general restricted SOS model where both the couplings considered in Refs. 11 and 18 are included. The spin-1/2 model is, in all cases, a Heisenberg chain with $S_i^zS_j^z$ competing antiferromagnetic interactions ranging up to third neighbors. Secondly, we unambiguously show that the dimer-phase scenario is realized in the disordered flat phase, and discuss in detail the surface physics implications of such a scenario. Long-range dimer order suggests (see Sec. IV) a particular type of long-range order for the correlation function between (2×1) steps, and also between *local surface maxima*. In particular, one is led to study an order parameter P_{BW} — previously introduced by Bernasconi and Tosatti[12] — which measures the difference in the number of local surface maxima belonging to the white and the black sublattice of a fcc (110). Due to ''shadowing,'' or to surface lattice contraction, this order parameter is related to antiphase scattering intensity of He atoms of x rays, respectively, and is thus a quantity of direct interest. (See Sec. V.) P_{BW} is studied by finite-size analysis of classical Monte Carlo data, and found to be nonzero in the disordered flat phase of both the K_3 and K_4 model. It has a nonmonotonic temperature behavior, vanishing only at preroughening and in the rough phase.

The present paper is organized as follows. Section II introduces the BCSOS type of models that we consider. In Sec.

III we show in detail how these models may be mapped onto quantum spin-1/2 chain problems. In Secs. IV and V we discuss the phase diagrams as well as the physics of a ''dimer'' disordered flat phase. In Sec. VI we present the results of our Monte Carlo simulations and discuss possible experimental signatures of a dimer phase. SectionI VII, finally, contains some concluding remarks as well as a discussion of open problems.

II. RESTRICTED SOLID-ON-SOLID MODELS FOR A fcc (110) METAL SURFACE

The (110) surface of a fcc lattice is comprised of two interpenetrating rectangular sublattices of lattice constants $a_x=\sqrt{2}a_y$, which we will conventionally refer to as the white (W) and the black (B) sublattice. The surface lattice basis vectors are $\mathbf{x}=a_x\hat{\mathbf{x}}$ and $\mathbf{y}=a_y\hat{\mathbf{y}}$, where $\hat{\mathbf{x}}=(001)$, and $\hat{\mathbf{y}}=(1\bar{1}0)$. In the ideal unreconstructed (110) surface, one of the two sublattices lies above the other at a distance $a_z=a_y/2$. Within a SOS framework,[21] one associates to each site $\mathbf{r}$ of the lattice a height variable $h_{\mathbf{r}}$, which can take only *integer* values (take $a_z=1$). The models we are going to study have an additional restriction, in that the height difference between each site and its four nearest neighbors (belonging to the other sublattice) is forced to be $\Delta h=\pm 1$. A height difference of 0 is therefore excluded, as well as larger values of Δh (they are energetically more costly). As a consequence, the values of $h_{\mathbf{r}}$ are forced to have opposite parity on the two sublattices, say even on W and odd on B. This restriction is typical of the BCSOS model.[17] It is probably justified for a metal, where strong inward relaxation makes the first and second layer bonds extra strong. On the contrary, it should not be expected to hold for, say, a rare-gas solid (110) face, where these bonds are in fact weaker.

Our Hamiltonian is written as

$$\mathscr{H}=\mathscr{H}_{\mathrm{BCSOS}}+\Delta\mathscr{H}, \tag{1}$$

where $\mathscr{H}_{\mathrm{BCSOS}}$ describes interactions between sublattice nearest neighbors, and $\Delta\mathscr{H}$ takes into account further-neighbor interactions, which will favor or disfavor reconstructed phases. Specifically, $\mathscr{H}_{\mathrm{BCSOS}}$ is given by

$$\mathscr{H}_{\mathrm{BCSOS}}=K_{2y}\sum_{\mathbf{r}}(h_{\mathbf{r}+\mathbf{y}}-h_{\mathbf{r}})^2+K_{2x}\sum_{\mathbf{r}}(h_{\mathbf{r}+\mathbf{x}}-h_{\mathbf{r}})^2, \tag{2}$$

with different coupling strengths in the two directions to take into account the anisotropy of the surface. K_{2y} will be always assumed to be *positive* and is generally the largest energy in the problem. The correspondent physics is that it is very costly to create a kink on a tightly packed (110) row. The absolute value of K_{2x}, i.e., of the coupling between rows, is instead much smaller, since atoms in neighboring rows are only second bulk neighbors. For $K_{2x}>0$, the (110) surface is stable in its (1×1) unreconstructed form. If $\Delta\mathscr{H}=0$ we recover the BCSOS model, which is exactly solved through a mapping to the six-vertex model,[17] and shows a *single transition*. This is of the Kosterlitz-Thouless type, between a low-temperature ordered (unreconstructed) flat phase and a high-temperature disordered rough phase. For $K_{2x}<0$ the surface becomes unstable against (110) step formation. In this case the final stable state is determined by

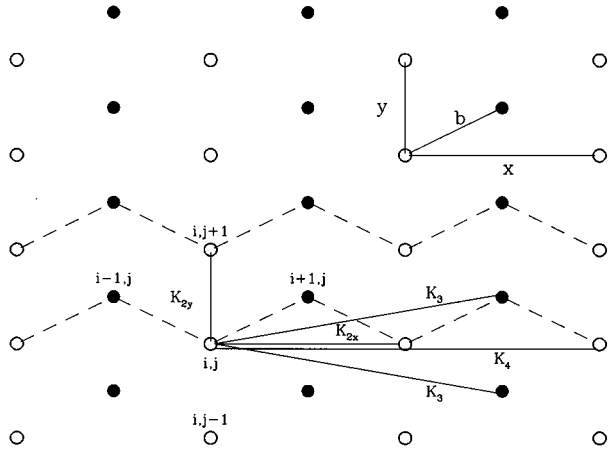

FIG. 1. Schematic top view of the fcc (110) surface. The two sublattices, W and B, are denoted by open and solid circles. In the ideal unreconstructed (110) surface, one of the two sublattices lies at a distance $a_z=a_y/2$ above the other. The couplings considered in the model are indicated. Lattice basis vectors are also shown. The dashed zig-zag lines represent successive row configurations (''time slices'') used in the spin-chain mapping.

more distant interactions, contained in $\Delta\mathscr{H}$. As for $\Delta\mathscr{H}$, two possible simple choices have been made in the literature, corresponding to what we will refer to as the ''K_3 model'' and the ''K_4 model.'' The K_3 model has been introduced by Mazzeo *et al.*,[11] and is defined by

$$\Delta\mathscr{H}_{(K_3)}=\frac{K_3}{2}\sum_{\mathbf{r}}[(h_{\mathbf{r}+\mathbf{x}+\mathbf{b}}-h_{\mathbf{r}})^2+(h_{\mathbf{r}+\mathbf{x}-\mathbf{y}+\mathbf{b}}-h_{\mathbf{r}})^2], \tag{3}$$

with $K_3\geq 0$, and $\mathbf{b}=(\mathbf{x}+\mathbf{y})/2$ (see Fig. 1). The introduction of this further-neighbor interaction stabilizes the (2×1) MR reconstructed phase.[11] In fact, it is very easy to check that $K_{2x}<0$, $K_3>0$ stabilizes an ordered succession of up and down (110) steps, which is precisely the (2×1) MR state. An alternative way of stabilizing the same (2×1) MR state against (111) faceting is realized with the K_4 model, whose $\Delta\mathscr{H}$ reads

$$\Delta\mathscr{H}_{(K_4)}=K_4\sum_{\mathbf{r}}(h_{\mathbf{r}+2\mathbf{x}}-h_{\mathbf{r}})^2, \tag{4}$$

with $K_4\geq 0$. The fourth neighbor interaction in the x direction has the effect, once again, of increasing the energy of configurations with $|h_{\mathbf{r}+2\mathbf{x}}-h_{\mathbf{r}}|=4$. This model was originally proposed by Kohanoff and Tosatti,[22] and has been recently studied in detail in Ref. 18. More generally, we could include both types of couplings by taking

$$\Delta\mathscr{H}=\Delta\mathscr{H}_{(K_3)}+\Delta\mathscr{H}_{(K_4)}. \tag{5}$$

In subsequent calculations and simulations, the lattice will be taken to have $N_c=N_x\times N_y$ primitive cells, i.e., $2N_x\times N_y$ sites. Periodic boundary conditions are assumed in both directions. A schematic representation of the lattice and of the interactions considered is given in Fig. 1.

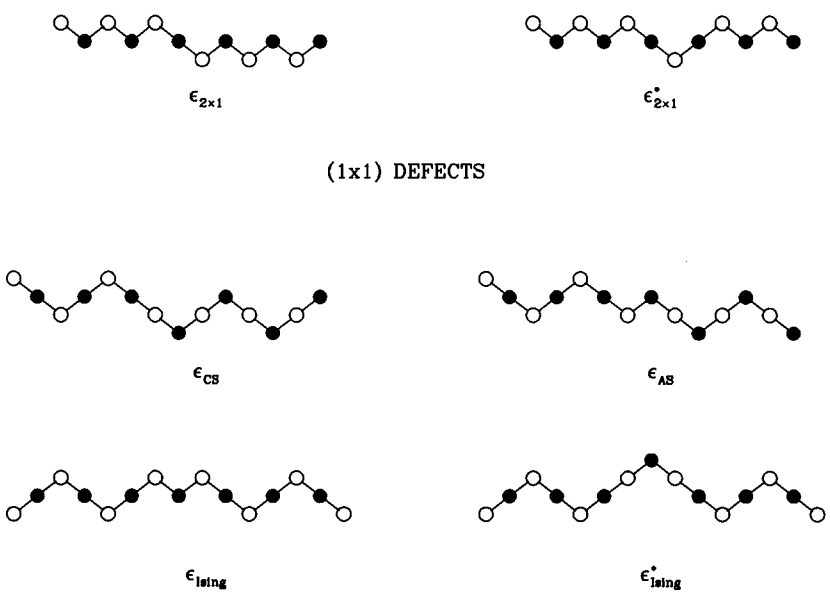

FIG. 2. Relevant extended defects (steps and walls) of a (1×1) and of a (2×1) reconstructed surface. The ground-state energies of these defects are given in Table I. $\epsilon_{2\times1}$ is the (2×1) (or monoatomic) step discussed in Sec. V. (2×1) steps proliferate in the DF phase, mantaining up-down long-range order. $\epsilon^{*}_{2\times1}$ is a bound pair of (2×1) steps, the relevant defect of an unreconstructed surface. $\epsilon_{\rm CS}$ and $\epsilon_{\rm AS}$ are clockwise [or (3×1)] and anticlockwise [or (1×1)] steps. $\epsilon_{\rm Ising}$ and $\epsilon^{*}_{\rm Ising}$ are two possible types of domain walls.

The classical $T=0$ ground states for both models are easy to work out as a function of the dimensionless ratio $\mathscr{K}=K_{2x}/K_3$ or $\mathscr{K}=K_{2x}/K_4$. For both models one finds that $\mathscr{K}>0$ corresponds to an unreconstructed ground state [or (1×1)], whereas for $-4<\mathscr{K}<0$ the ground state is (2×1) MR reconstructed.[11] For the sake of completeness, we mention that, for the K_3 model, the ground state degenerates into an infinite (111) large facet as soon as $\mathscr{K}<-4$.[11] For the K_4 model, on the contrary, an infinite (111) facet sets in only for $\mathscr{K}<-8$, and there is a whole series of intermediate regions $[(12-8n)/(n-1)<\mathscr{K}<(20-8n)/(n-2)$ with $n\geqslant3]$ where the ground state is $(n\times1)$ MR reconstructed. In the following we will be interested exclusively in the region of parameter space where the interplay between unreconstructed and (2×1) MR reconstructed phases takes place, hence $\mathscr{K}>-4$.

Neglecting adatoms, vacancies and (as necessary in SOS models) overhangs, the defects that should play a role in the disordering and roughening transitions are unbound steps and bound pairs of steps, i.e., Ising domain walls. Figure 2 illustrates the most relevant defects for both a (1×1) and a (2×1) surface. The ground-state energies of these defects are given, for both the K_3 and the K_4 model, in Table I. It is worth noting that the K_3 model has defects whose energy goes to zero as $K_{2x}\to0$. These are the (2×1) step and the $(2\times1)^*$ wall in the (1×1) case, and the anticlockwise step and the Ising wall in the (2×1) reconstructed case. Since this leads to zero-point entropy, the $K_{2x}\to0$ region is therefore somewhat unphysical for the K_3 model, where one might expect disorder to occur at very low temperatures.[23] As a second point, we observe that in the K_4 model a combination of two Ising walls wins against combinations involving clockwise steps for $\mathscr{K}=K_{2x}/K_4>-1$, while it always wins against anticlockwise steps. In principle, therefore, a DEF (wall dominated) phase seems to be plausible for $-1<\mathscr{K}<0$ in the K_4 model. Later on we will present results that show how ground-state defect energy considerations can be somewhat misleading: the disordered phase obtained does not have the features of an ideal DEF.

III. MAPPING INTO A QUANTUM SPIN-$\frac{1}{2}$ CHAIN

An elegant and convenient way of studying the temperature phase diagram of the classical two-dimensional models introduced in the previous section consists in mapping them into one-dimensional quantum problems.[19] The general procedure is well known,[19,24,25] but we review it here for our specific case, and for the reader's convenience.

The method consists in viewing the y direction of the lattice as the (imaginary) time direction of an appropriate 1D quantum problem, different row configurations in the x direction being viewed as subsequent time slices for the quantum problem. The physical requirement that will turn out to be important is that the coupling K_{2y} in the y direction is strong, while the other couplings are much weaker (strong anisotropy limit). The starting point for the mapping is a transfer matrix formulation of the classical partition function $\mathscr{Z}$. The notation $\mathbf{r}=(i,j)$ (and $h_{\mathbf{r}}=h_i^{(j)}$) for the lattice sites used in the present section is illustrated in Fig. 1: the value of j, the time-slice index, is the same along each dashed zig-zag line shown in Fig. 1; within each zig-zag line, the W and the B sublattices are characterized, respectively, by even and odd values of i. The classical partition function is given by

$$\mathscr{Z}=\sum_{\{h_i^{(j)}\}} e^{-\beta\mathscr{H}}=\sum_{h^{(1)}}\cdots\sum_{h^{(N_y)}}\langle h^{(1)}|\hat{T}|h^{(N_y)}\rangle\cdots\langle h^{(3)}|\hat{T}|h^{(2)}\rangle \times\langle h^{(2)}|\hat{T}|h^{(1)}\rangle, \tag{6}$$

where $|h^{(j)}\rangle=\{h_i^{(j)}:i=1,\ldots,N_s\}$ is the jth *row configuration* (a dashed zig-zag line in Fig. 1, containing $N_s=2N_x$ sites), and $\hat{T}$ is the classical transfer matrix. Periodic boundary conditions have been used in the y direction, and are understood in the x direction. It is also understood that con-

figurations differing by a uniform shift of the heights should be included only once in the partition sum. For the models we are considering, the transfer matrix elements read

$$\langle h^{(j+1)}|\hat{T}|h^{(j)}\rangle = B_{nn}\exp\Bigg\{-\beta K_{2y}\sum_{i=1}^{N_s}(h_i^{(j+1)}-h_i^{(j)})^2 - \beta K_{2x}\sum_{i=1}^{N_s}(h_{i+2}^{(j)}-h_i^{(j)})^2\Bigg\}, \tag{7}$$

where B_{nn} is the Boltzmann weight contribution due to further neighbor interactions. For the K_3 model, B_{nn} is given by

$$B_{nn}^{(K_3)} = \exp\Bigg\{-\frac{\beta K_3}{2}\sum_{i\ \text{even}}^{N_s}[(h_{i+3}^{(j)}-h_i^{(j)})^2+(h_{i+3}^{(j)}-h_i^{(j+1)})^2]\Bigg\} \times\exp\Bigg\{-\frac{\beta K_3}{2}\sum_{i\ \text{odd}}^{N_s}[(h_{i+3}^{(j)}-h_i^{(j)})^2 + (h_{i+3}^{(j+1)}-h_i^{(j)})^2]\Bigg\}, \tag{8}$$

whereas for the K_4 model the result is

$$B_{nn}^{(K_4)} = \exp\Bigg\{-\beta K_4\sum_{i=1}^{N_s}(h_{i+4}^{(j)}-h_i^{(j)})^2\Bigg\}. \tag{9}$$

For the model in which both couplings are present, one clearly has

$$B_{nn} = B_{nn}^{(K_3)}B_{nn}^{(K_4)}. \tag{10}$$

Notice that in the partition function, Eq. (6), it is implicitly assumed that the configurations included have to fulfill the BCSOS constraint $\Delta h = \pm 1$ for nearest neighbors. As a consequence, within each row we must have $h_{i+1}^{(j)} - h_i^{(j)} = \pm 1$. Therefore, we can associate to any row configuration $|h^{(j)}\rangle$ a state $|j\rangle$ in the Hilbert space of a quantum spin-$\frac{1}{2}$ chain (of length N_s) by the relationship

$$|h^{(j)}\rangle \rightarrow |j\rangle = |S_1, S_2, \ldots, S_{N_s}\rangle,$$

$$S_i = \tfrac{1}{2}(h_{i+1}^{(j)} - h_i^{(j)}). \tag{11}$$

(In doing so we lose information on the absolute height of the surface, which is, however, irrelevant in a static context.) Figure 3 illustrates the explicit mapping of the (1×1) and (2×1) ground states in terms of spin configurations.

The idea is now to reproduce the Boltzmann factors appearing in the matrix elements of the classical transfer matrix $\langle h^{(j+1)}|\hat{T}|h^{(j)}\rangle$ by a suitable quantum operator T_Q in the spin Hilbert space, i.e.,

$$\langle h^{(j+1)}|\hat{T}|h^{(j)}\rangle = \langle j+1|T_Q|j\rangle, \tag{12}$$

where $|j\rangle$ and $|j+1\rangle$ are the quantum spin states corresponding to $|h^{(j)}\rangle$ and $|h^{(j+1)}\rangle$, respectively. In certain cases, the exact expression for the quantum operator T_Q can be worked out quite easily. T_Q for the K_4 model has been derived in Ref. 18. The exact T_Q is, however, of no practical use, being a product of noncommuting terms involving spin-$\frac{1}{2}$ operators. The crucial step that makes the whole mapping useful is the so-called *time-continuum limit* or *strong anisotropy limit*.

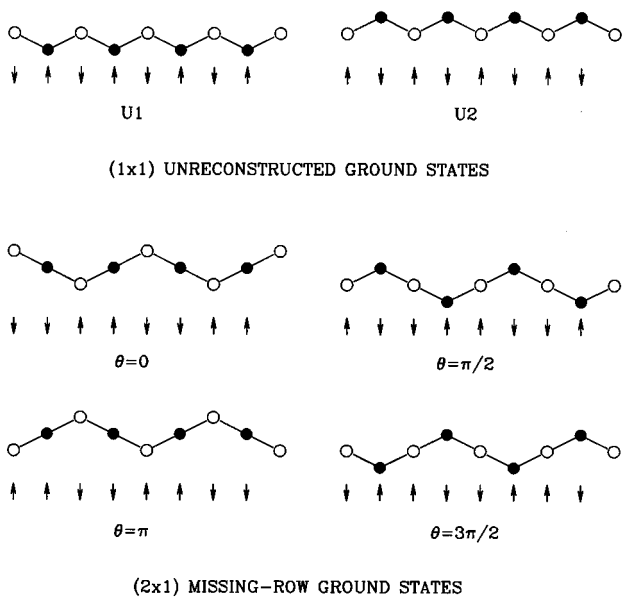

FIG. 3. Schematic height profiles of the two ground states ($U1$ denotes white, $U2$ denotes black) of the unreconstructed surface, and of the four ground states of the (2×1) missing-row surface. The reconstruction variable θ is indicated. The spin representation of each state, using Eq. (11), is given explicitly. Notice that the two unreconstructed ground states correspond to the two possible Néel states of a spin-$\frac{1}{2}$ chain.

Physically, one assumes that the ''time'' direction coincides with the ''hard'' direction of the classical problem, i.e., that the coupling in the y direction is much stronger than the other couplings. This is plausibly the case for the fcc (110) surface, where the $\hat{\mathbf{y}} = (1\bar{1}0)$ direction is hard, and the $\hat{\mathbf{x}} = (001)$ direction is soft, as discussed above. Anisotropy, moreover, is not expected to play any role in the qualitative shape of the phase diagram.[15]

In the strong anisotropy limit the quantum operator T_Q will reduce to the imaginary-time evolution operator $e^{-\tau H_S}$ for a suitable Hamiltonian H_S, with $\tau\rightarrow0$. To find H_S, assume βK_{2y} to be large, so that $e^{-4\beta K_{2y}} = (J/2)\tau$, τ being a small quantity (and J of order one). Assume also all the other couplings to be small and proportional to τ, i.e., $\beta K_{2x} \propto \tau$, $\beta K_3 \propto \tau$, and $\beta K_4 \propto \tau$. We need a spin Hamiltonian H_S such that Eq. (12) is verified with

$$T_Q \approx e^{-\tau H_S} \approx 1 - \tau H_S + O(\tau^2), \tag{13}$$

up to first order in the small quantity τ. A diagonal matrix elements of $\hat{T}$ reads, using Eqs. (7)–(10),

$$\langle h^{(j)}|\hat{T}|h^{(j)}\rangle = 1 - \beta K_{2x}\sum_i (h_{i+2}^{(j)}-h_i^{(j)})^2 - \beta K_3\sum_i (h_{i+3}^{(j)}-h_i^{(j)})^2 - \beta K_4\sum_i (h_{i+4}^{(j)}-h_i^{(j)})^2 + O(\tau^2), \tag{14}$$

where we have expanded all the exponentials up to first order in small quantities ($\propto\tau$). The first requirement for H_S is that its diagonal terms must give the same result, i.e., using Eqs. (13), (14), and (11),

$$\begin{aligned}\langle j|T_Q|j\rangle &\approx 1-\tau\langle j|H_S|j\rangle+O(\tau^2)\\ &=1-4\beta K_{2x}\sum_i\,(S_i+S_{i+1})^2\\ &\quad-4\beta K_3\sum_i\,(S_i+S_{i+1}+S_{i+2})^2\\ &\quad-4\beta K_4\sum_i\,(S_i+S_{i+1}+S_{i+2}+S_{i+3})^2+O(\tau^2).\end{aligned}\tag{15}$$

An *off-diagonal* matrix element of $\hat{T}$ must contain a Boltzmann factor $e^{-4\beta K_{2y}}=(J/2)\tau$, for each site i such that $h_i^{(j+1)}=h_i^{(j)}\pm 2$. Therefore, up to first order in τ we need to consider only row configurations $h^{(j+1)}$ that differ from $h^{(j)}$ only at a single site i. Let $\{\ldots,h_{i-1},h_i,h_{i+1},\ldots\}$ be the local configuration of row j around such a site i. It is easy to realize that, in order to satisfy the BCSOS constraint with $h_i^{(j+1)}=h_i^{(j)}\pm 2$, and $h_k^{(j+1)}=h_k^{(j)}$ for $k\neq i$, the only possibility is to have $h_{i-1}^{(j)}=h_{i+1}^{(j)}=h_i^{(j)}\pm 1$, i.e.,

$$\begin{aligned}|h^{(j)}\rangle&=\{\ldots,h_i\pm 1,h_i,h_i\pm 1,\ldots\}\\ &\rightarrow|h^{(j+1)}\rangle=\{\ldots,h_i\pm 1,h_i\pm 2,h_i\pm 1,\ldots\}\ .\end{aligned}$$

In terms of the corresponding spin configurations, this simply leads to a *spin flip* of the spins at sites $i-1$ and i,

$$\begin{aligned}|j\rangle&=|\ldots,S_{i-1}=\mp\tfrac{1}{2},S_i=\pm\tfrac{1}{2},\ldots\rangle\rightarrow|j+1\rangle\\ &=|\ldots,S_{i-1}=\pm\tfrac{1}{2},S_i=\mp\tfrac{1}{2},\ldots\rangle.\end{aligned}$$

The corresponding $\hat{T}$-matrix element reads, up to first order in τ,

$$\langle h^{(j+1)}|\hat{T}|h^{(j)}\rangle=e^{-4\beta K_{2y}}[1+O(\tau)]\approx-\tau\langle j+1|H_S|j\rangle.\tag{16}$$

It is easy to verify, in conclusion, that the correct form of H_S verifying Eqs. (15) and (16) is given, neglecting an overall constant, by

$$\begin{aligned}H_S=-\frac{J}{2}\sum_{i=1}^{N_s}[S_i^+S_{i+1}^-+S_i^-S_{i+1}^+]+\sum_{i=1}^{N_s}[J_zS_i^zS_{i+1}^z+J_2S_i^zS_{i+2}^z\\ +J_3S_i^zS_{i+3}^z],\end{aligned}\tag{17}$$

where the spin couplings are related to the original couplings as follows:

$$\begin{aligned}\tau J&=2\exp(-4\beta K_{2y}),\\ \tau J_z&=8\beta(K_{2x}+2K_3+3K_4),\\ \tau J_2&=8\beta(K_3+2K_4),\\ \tau J_3&=8\beta K_4.\end{aligned}\tag{18}$$

Indeed, the spin-flip part of H_S reproduces the off-diagonal matrix element in Eq. (16), whereas the S^zS^z terms give rise to the correct diagonal matrix element in Eq. (15).

It is well known that this kind of mapping is such that the free energy per site of the classical problem — given by the maximum eigenvalue of the transfer matrix — is related to the ground-state energy per site of the one-dimensional quantum problem, $\beta f=\tau\epsilon_{\rm GS}$.[24] The temperature clearly enters through the spin couplings, see Eq. (18), so that any genuine singularity of the classical free energy versus temperature can be seen as a ground-state energy singularity for the quantum problem as a function of the couplings J_z/J, J_2/J, and J_3/J. Moreover, temperature averages for correlation functions of the classical problem can be likewise rewritten in the form of ground-state averages for the corresponding quantum correlation function.[24] In summary, to obtain information about the temperature phase diagram of the classical model one studies the *ground-state phase diagram* of the spin chain model.[26]

Before entering into the discussion of the phase diagram, let us clarify that the quantum mapping not only gives the correct *critical behavior* of the transitions (if anisotropy is not ''relevant'' in the renormalization-group sense), but provides also *quantitative* results on the transition temperatures that are expected to be quite good even if the anisotropy is in reality only weak. As a simple check of this point, consider the exactly solvable BCSOS case, whose transition temperature is given by Ref. 17

$$e^{-4\beta_cK_{2y}}+e^{-4\beta_cK_{2x}}=1.\tag{19}$$

The BCSOS model maps — see Eq. (18) — into the nearest-neighbor XXZ Heisenberg chain, which is known to have a KT transition at the isotropic point $J_z=J$.[20] Using Eq. (3), this readily implies a predicted transition temperature $\beta_c^{(Q)}$ satisfying

$$e^{-4\beta_c^{(Q)}K_{2y}}=4\beta_c^{(Q)}K_{2x}.\tag{20}$$

Figure 4 shows both the exact (solid line) and the quantum mapping transition temperature (dashed line) for the BCSOS as a function of the anisotropy ratio K_{2x}/K_{2y}. The results agree within a few percent even for rather weak anisotropies, such as $K_{2x}/K_{2y}=0.2$, and remain reasonable all the way to the full isotropic case, $K_{2x}/K_{2y}=1$.

IV. PHASE DIAGRAMS

A. Phase diagram of the spin-$\frac{1}{2}$ chain

The spin chain Hamiltonian corresponding to our modified BCSOS model is a Heisenberg XXZ model with a second-neighbor and a (less important) third-neighbor $S_i^zS_j^z$ coupling

$$\begin{aligned}H_S=-\frac{J}{2}\sum_{i=1}^{N}[S_i^+S_{i+1}^-+S_i^-S_{i+1}^+]\\ +\sum_{i=1}^{N}[J_zS_i^zS_{i+1}^z+J_2S_i^zS_{i+2}^z+J_3S_i^zS_{i+3}^z].\end{aligned}\tag{21}$$

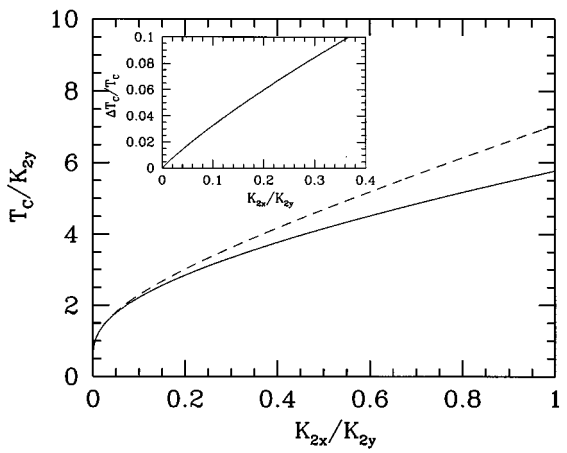

FIG. 4. The exact roughening temperature of the anisotropic BCSOS model (solid line) and the result obtained by making use of the mapping onto the *XXZ* Heisenberg chain (dashed line), as a function of the anisotropy ratio K_{2x}/K_{2y}. The inset shows the relative discrepancy between the two results.

Qualitatively — and for not too large values of the couplings J_z, J_2, J_3 — the physics of such a model is closely related to that of the Heisenberg chain with spin-isotropic second-neighbor interactions,

$$H=\frac{J}{2}\sum_i\ [S_i^+S_{i+1}^-+S_i^-S_{i+1}^+]+\sum_i\ [J_zS_i^zS_{i+1}^z+J_2\vec{S}_i\cdot\vec{S}_{i+2}], \tag{22}$$

which we will refer to, in the following, as the $J-J_2$ model.[27] Haldane has discussed the qualitative phase diagram of the $J-J_2$ model in the context of the Luttinger liquid framework, with special emphasis on the role played by umklapp processes in the underlying spinless fermion problem.[20] (For a detailed quantitative analysis see Ref. 28.) For the spin model in Eq. (21), the discussion goes along similar lines. For completeness we will give in Sec. IV C some details of this analysis based on standard techniques of one-dimensional systems.[20,29]

Even a simple mean-field treatment, however, is quite instructive about the nature of the ordered phases that are to be expected. The starting point is to perform a Wigner-Jordan transformation from spin variables to spinless fermion operators c_i, i.e., $S_i^z=c_i^\dagger c_i-1/2$, $S_i^+=c_i^\dagger\exp(i\pi\Sigma_{j<i}n_j)$. Neglecting constants and terms proportional to the total number of fermions, the spin model is then rewritten as the following *spinless fermion* model

$$\begin{aligned}H_F&=-t\sum_{i=1}^N\ [c_i^\dagger c_{i+1}+c_{i+1}^\dagger c_i]\\&\quad+\sum_{i=1}^N\ [J_zn_in_{i+1}+J_2n_in_{i+2}+J_3n_in_{i+3}]\\&=\sum_k^{BZ}\ \epsilon_kc_k^\dagger c_k+\frac{1}{N}\sum_q^{BZ}\ v(q)\rho(q)\rho(-q),\end{aligned} \tag{23}$$

where $c_k=N^{-1/2}\Sigma_je^{-ikaj}c_j$, with k belonging to the first Brillouin zone $[-\pi/a,\pi/a]$ (BZ), and $\rho(q)$ is the Fourier transform of the fermion density operator, $\rho(q)=\Sigma_kc_k^\dagger c_{k+q}$. Here $\epsilon_k=-2t\cos(ka)$ with $t=J/2$, and $v(q)$ is the Fourier transform of the interaction potential, $v(q)=J_z\cos(qa)+J_2\cos(2qa)+J_3\cos(3qa)$. Since $\Sigma_iS_i^z=\Sigma_in_i-N/2$, zero total magnetization for the spin system implies half filling for the fermions, i.e., a Fermi surface consisting of two Fermi points at $\pm k_F$, with $k_Fa=\pi/2$. In the absence of interaction ($J_z=J_2=J_3=0$, i.e., the *XY* spin chain) we have a simple free-fermion problem. The two Fermi points induce nesting with a wave vector $2k_F=\pi/a$, a hint that the system would tend to open up a gap at the Fermi surface by developing long-range order (LRO) with wave vector π/a and making the average $A_k=\langle c_{k+\pi/a}^\dagger c_k\rangle$ different from zero. A standard mean-field factorization of the quartic term in Eq. (23), assuming $\langle c_{k+\pi/a}^\dagger c_k\rangle\neq0$, leads to the following mean-field Hamiltonian (we take $a=1$ from now on):

$$H_F^{\rm MF}=\sum_k^{\rm RBZ}\ \widetilde{\epsilon}_k[c_k^\dagger c_k-c_{k+\pi}^\dagger c_{k+\pi}]+[\Delta_kc_k^\dagger c_{k+\pi}+\text{H.c.}], \tag{24}$$

where $\widetilde{\epsilon}_k=\epsilon_k-(2/N)\Sigma_{k'\in\rm BZ}v(k-k')\langle c_{k'}^\dagger c_{k'}\rangle$, and $\Delta_k=(2/N)\Sigma_{k'\in\rm BZ}[v(\pi)-v(k-k')]\langle c_{k'+\pi}^\dagger c_{k'}\rangle$. Here RBZ stands for the reduced magnetic Brillouin zone $(-\pi/2,\pi/2)$. Diagonalizing the simple 2×2 problem appearing in $H_F^{\rm MF}$, one readily finds that the ''anomalous'' average $A_k=\langle c_{k+\pi}^\dagger c_k\rangle$ is simply related to Δ_k, $A_k=-\Delta_k/(2E_k)$ with $E_k=\sqrt{\widetilde{\epsilon}_k^2+|\Delta_k|^2}$, and that $\widetilde{\epsilon}_k$ and Δ_k have to obey the self-consistency conditions

$$\begin{aligned}\widetilde{\epsilon}_k&=\epsilon_k+\frac{1}{N}\sum_{k'}^{\rm RBZ}\ [v(k-k')-v(k-k'+\pi)]\frac{\widetilde{\epsilon}_{k'}}{E_{k'}},\\\Delta_k&=-\frac{1}{N}\sum_{k'}^{\rm RBZ}\ \frac{1}{E_{k'}}\{[v(\pi)-v(k-k')]\Delta_{k'}\\&\quad+[v(\pi)-v(k-k'+\pi)]\Delta_{k'}^*\}.\end{aligned} \tag{25}$$

Let us consider, for definiteness, the case $J_3=0$. Solving the self-consistency equations (25), one finds that if $v(\pi)=J_2-J_z$ is sufficiently negative (J_2 less than $\approx0.4J_z$), Δ_k is *real* and has the form $\Delta_k=\delta_0+\delta_2\cos(2k)$. Upon increasing J_2, a transition occurs to a phase in which Δ_k is *purely imaginary*, $\Delta_k=i\delta_1\sin(k)$. The transition appears to be first order in mean field. To understand the meaning of the two phases, consider the average values of the fermion density $\langle n_i\rangle$, and of the bond kinetic energy $\langle c_i^\dagger c_{i+1}+c_{i+1}^\dagger c_i\rangle$. A simple calculation shows that

$$\begin{aligned}\langle n_i\rangle&=\frac{1}{2}-(-1)^i\frac{1}{N}\sum_k^{\rm RBZ}\ \frac{\text{Re}\Delta_k}{E_k},\\\langle c_i^\dagger c_{i+1}+c_{i+1}^\dagger c_i\rangle&=\text{const}+(-1)^i\frac{2}{N}\sum_k^{RBZ}\ \sin(k)\frac{\text{Im}\Delta_k}{E_k}.\end{aligned} \tag{26}$$

The phase with Δ_k real (small J_2) is therefore a $2k_F$ *site-centered charge-density wave* (CDW) [i.e., a Néel phase with $\uparrow\downarrow\uparrow\downarrow$ LRO in the spin language, or an ordered fcc (110) face in the surface language], whereas the phase at larger

J_2, with Δ_k purely imaginary, is a $2k_F$ *bond-centered charge-density wave*. We can picture the latter by assuming that on every other bond the fermions are in a state that maximizes the kinetic energy of the bond,

$$\Psi_{\text{bond CDW}}=\prod_{i\,\text{even}}\frac{(c_i^\dagger+c_{i+1}^\dagger)}{\sqrt{2}}|0\rangle, \tag{27}$$

as opposed to the ideal site-CDW state (the Néel state $\uparrow\downarrow\uparrow\downarrow$)

$$\Psi_{\text{site CDW}}=\prod_{i\,\text{even}} c_i^\dagger|0\rangle. \tag{28}$$

The spin interpretation of the bond-centered CDW state is quite obviously a dimerized spin state with every other bond engaged in a singlet $(\uparrow\downarrow-\downarrow\uparrow)$.[27] Unlike the site-centered CDW, where every second neighbor is occupied and pays an energy J_2, a bond-centered CDW reduces the second-neighbor average occupancy to about 1/2, and is thus favored upon increasing J_2. As will be discussed in detail, this spin dimer phase corresponds to a disordered flat phase in the surface language. Clearly, for very large J_2, the system will eventually prefer to minimize second-neighbor occupancies by forming a site-centered CDW of double periodicity (i.e., a k_F CDW), which we can picture as

$$\Psi_{k_F\text{CDW}}=\prod_{i=4n} c_i^\dagger c_{i+1}^\dagger|0\rangle. \tag{29}$$

[Such a state corresponds to $\uparrow\uparrow\downarrow\downarrow$ LRO in spin language, or a (2×1) MR reconstructed face in the surface language.] This phase can be included in a mean-field treatment by allowing, in the factorization of the quartic term, anomalous averages of the type $\langle c_{k\pm\pi/2}^\dagger c_k\rangle$, as well as the previous one $\langle c_{k+\pi}^\dagger c_k\rangle$.

A finite-size scaling study of the spin model readily confirms most of the qualitative features of the mean-field phase diagram. A quantitative phase diagram for the spin model corresponding to the K_3 model, i.e., Eq. (21) with $J_3=0$, is presented in Fig. 5. The procedure to obtain such a phase diagram from a finite-size scaling study of chains up to $N=28$ sites[30] was described in detail in Ref. 18. (See also Ref. 28.) A similar phase diagram for the spin chain corresponding to the K_4 model, i.e., Eq. (21) with $J_3=J_2/2$, was presented in Fig. 1 of Ref. 18. For the purpose of a general discussion, we reproduce in Fig. 6 the essential qualitative features of the spin chain phase diagram for a generic $J_3=\alpha J_2$ with $0<\alpha\leqslant1/2$. The model has a spin liquid XY-like phase at small J_2 and J_z, which corresponds, in the fermion language, to a spinless Luttinger liquid characterized by a certain Luttinger exponent K. (See Sec. IV C for more details on this discussion.) At a given universal value of the Luttinger exponent ($K=1/2$), the Luttinger liquid phase becomes unstable — because of *umklapp processes* — against two different (gapped) ordered phases, depending on the sign of the effective coupling of the umklapp term: a Néel phase with $\uparrow\downarrow\uparrow\downarrow$ LRO, for large J_z and small J_2, and a dimer phase, for larger J_2. Both phases have a *gap* in the excitation spectrum, and a *doubly degenerate* ground state that *breaks translational symmetry*.[20,28] These two ordered phases are separated by a critical line of continuously varying exponent, labeled PM in Fig. 6, along which the effective coupling of the umklapp term vanishes and the system behaves as a Luttinger model with a Luttinger exponent $1/8<K<1/2$. Beyond the point M in Fig. 6, the nature of the line changes from nonuniversal to first order. For even larger values of J_2 the other ordered phase, with spins acquiring $\uparrow\uparrow\downarrow\downarrow$ LRO and a fourfold degenerate ground state, wins over the dimer phase. This is the only feature of Figs. 5 and 6 that is qualitatively new with respect to the phase diagram of the $J-J_2$ model [Eq. (22)].[31]

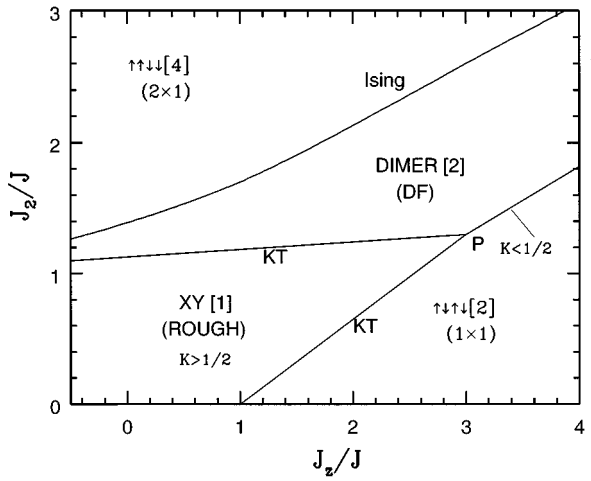

FIG. 5. Ground-state phase diagram of the Heisenberg chain with second-neighbor $S_i^zS_{i+2}^s$ coupling. Ground-state degeneracies are given in square brackets, and the translation of the different phases in the surface language is explicitly indicated. The (1×1) DF line starting at the point P is continuous, with a variable exponent.

The nature of the line separating the $\uparrow\uparrow\downarrow\downarrow$ phase from the dimer phase is an open issue. Previous studies of the K_3 model[11] and of the spin chain[18] found exponents that appeared to be compatible with the 2D Ising universality class. Recently, a transfer matrix study of a 2D model closely re-

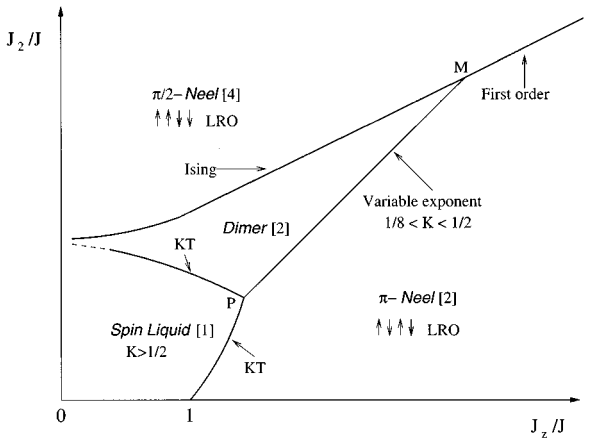

FIG. 6. Qualitative ground-state phase diagram for the Heisenberg chain with second- and third-neighbor $S_i^zS_j^s$ couplings, for $J_3=\alpha J_2$ with $0<\alpha\leqslant1/2$. Ground-state degeneracies are given in square brackets. The line labeled PM has a variable exponent.

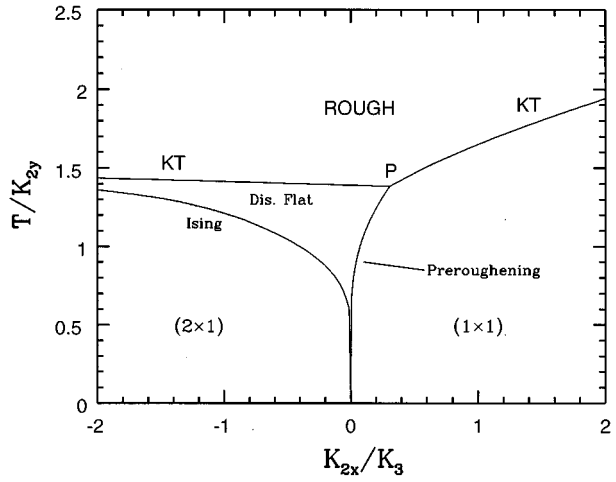

FIG. 7. Phase diagram for the K_3 model, as obtained from the quantum spin-chain mapping, for $K_3/K_{2y}=0.025$.

lated to the K_4 model has found exponents that are incompatible with Ising.[32] Moreover, a transfer matrix study of a two-component BCSOS model has found deviations from Ising, possibly related to a crossover to Ising behavior not accessible by finite-size strips ($N_{\rm strip}<22$), when the critical line approaches a KT line.[33] A definite answer to the nature of this transition, possibly connected to the presence or absence of the multicritical point M in the phase diagram,[32] needs further study. In spite of this uncertainty, we will continue to refer to this line, for convenience, as ''Ising.''

A second open issue concerns the region of the phase diagram where the KT line and the Ising line seem to approach each other. A relevant question, which we have not been able to answer, is whether the KT and the Ising lines actually merge, and, if so, what is the nature of the resulting line.

B. Phase diagram of the modified BCSOS models

The translation of Fig. 5 into a temperature phase diagram for K_3 model, using Eqs. (18), is shown in Fig. 7.[26] The generic phase diagram of our modified BCSOS model, in the (T,K_{2x}) plane for given values of K_3 and K_4, is qualitatively sketched in Fig. 8.[23] Four phases are found in a region of parameters relevant to the unreconstructed and (2×1) MR reconstructed case. At very high temperatures, there is a rough phase. It corresponds, in the spin problem, to the region close to XY-model point $(J_z=J_2=J_3=0)$ in which spin-spin correlation functions decay as power laws at large distances (the Luttinger liquid or Gaussian model, see Sec. IV C). A large-distance uniform term of the type $-K/(2\pi^2n^2)$ in the spin-spin correlation function $\langle S_0^z S_n^z\rangle$ — see Eq. (41) — implies a logarithmic divergent height-height correlation function $G(n)=\langle[h_n^{(0)}-h_0^{(0)}]^2\rangle$, signaling a rough phase. Indeed, using Eq. (11) and translational invariance of the spin-spin correlation function, one verifies that

$$G(n)=\langle[h_n^{(0)}-h_0^{(0)}]^2\rangle=4\sum_{i,j=0}^{n-1}\langle S_i^z S_j^z\rangle$$
$$=n+8\sum_{i=1}^{n}(n-i)\langle S_0^z S_n^z\rangle=\frac{4K}{\pi^2}\ln(n)+\cdots,\quad n\to\infty. \tag{30}$$

At low temperatures, corresponding to large values of J_z/J and/or J_2/J in the spin-chain problem, a (1×1) and a (2×1) ordered phase are present for $K_{2x}>0$ and $K_{2x}<0$, respectively. The (1×1) and (2×1) ordered phases correspond, respectively, to $\uparrow\downarrow\uparrow\downarrow$ and $\uparrow\uparrow\downarrow\downarrow$ LRO for the spins (see Fig. 3). The other phase appearing in Figs. 7 and 8 is a disordered flat (DF) phase. It corresponds, in the spin language, to the dimer phase (see Sec. V for a more extensive discussion). The transition line from the (2×1) reconstructed phase to the DF phase is labeled ''Ising,'' in spite of the fact that its nature is not completely assessed (see previous section). The critical line separating the unreconstructed phase from the disordered flat phase has variable exponents: it is the *preroughening line*.[15] The parameter K appearing in Eq. (30) is the Luttinger exponent. In the rough phase $K>1/2$. Along the preroughening line correlation functions still behave as power laws with exponents related to K; Eq. (30) is still valid, with $1/8<K<1/2$.

C. Spinless Luttinger liquid and the variable exponent line

We now discuss in more detail how to extract, using standard techniques of one-dimensional systems, a qualitative phase diagram for our spin chain model and some useful information about the variable exponent line. The reader not interested in technical details might jump directly to the next section, where the surface interpretation of the dimer spin phase is discussed.

The starting point is the spinless fermion model in Eq. (23). The low-energy physics of such a model, as long as the interactions are not too strong, can be conveniently analyzed by going to the continuum limit, $a\to0$ with $Na=L$ fixed. One linearizes the fermionic band around the two Fermi points at $\pm k_F$, and introduces a right $(p=+)$ and a left $(p=-)$ branch of fermions, with fields $\psi_p(x)$.[34] All the interaction processes in which particles are scattered in the vicinity of the Fermi points are then classified in the so-called ''g-ology'' scheme.[29] The resulting *continuum* fermionic model $\mathscr{H}_F$ turns out to be a sum of two terms

$$\mathscr{H}_F=\mathscr{H}_{\rm Luttinger}+\mathscr{H}_{\rm umklapp}, \tag{31}$$

where $\mathscr{H}_{\rm Luttinger}$ is a spinless Luttinger model,[34]

$$\mathscr{H}_{\rm Luttinger}=v_F\sum_{p=\pm}\int_0^L dx{:}\psi_p^\dagger(x)[-ip\nabla-k_F]\psi_p(x){:}$$
$$+\sum_{p,p'=\pm}[g_4\delta_{p',p}+g_2\delta_{p',-p}]$$
$$\times\int_0^L dx{:}\rho_p(x)\rho_{p'}(x){:}, \tag{32}$$

and $\mathscr{H}_{\text{umklapp}}$ represents the crucial *umklapp processes*, i.e., processes where two fermions are scattered from the vicinity of one Fermi point to the opposite one,[29]

$$\mathscr{H}_{\text{umklapp}} = g_3 \int_0^L dx [:\psi_+^\dagger(x)\psi_-(x)\psi_+^\dagger(x)\psi_-(x): + \text{H.c.}]. \tag{33}$$

(Umklapp processes would not conserve the momentum for a general filling: at half-filling, however, momentum conservation is fulfilled modulo a reciprocal lattice vector, $G = 4k_F = 2\pi$.) Here $v_F = 2t = J$ is the Fermi velocity, and $\rho_p(x) = :\psi_p^\dagger(x)\psi_p(x):$ is the density operator for the p branch of fermions. (The $:\cdots:$ stands for a normal ordering procedure, as explained in Ref. 34.) Neglecting lattice renormalization effects we have, for the Luttinger couplings $g_4 = v(0) = (J_z + J_2 + J_3)$ and $g_2 = v(0) - v(\pi) = 2(J_z + J_3)$, whereas the umklapp coupling reads $g_3 = v(\pi) = (-J_z + J_2 - J_3)$. We stress the important point that *the sign of umklapp coupling g_3 results from a competition of J_z and J_2*. We will see that this fact is crucial to the existence of a line with variable exponents.

The final step is to *bosonize* the Hamiltonian in Eq. (31). This is achieved by introducing a bosonic representation of the fermionic fields[34,29]

$$\psi_p(x) = \frac{1}{\sqrt{2\pi\alpha}} \eta_p e^{ipk_F x} e^{ip\phi_p(x)}, \tag{34}$$

where α is a short-distance cutoff, and $\eta_p = \eta_p^\dagger$ are Majorana fermions ($\eta_p^2 = 1$) ensuring correct anticommutation properties among right- and left-moving fermions. The field $\phi_p(x)$ is related to the fermion density as follows:

$$\rho_p(x) = :\psi_p^\dagger(x)\psi_p(x): = \frac{1}{2\pi}\nabla\phi_p(x), \tag{35}$$

and is expressed in terms of standard boson operators $b_p(q)$ as

$$\phi_p(x) = \sum_{q>0} e^{-\alpha q/2}\left(\frac{2\pi}{Lq}\right)^{1/2} [e^{-ipqx} b_p^\dagger(q) + \text{H.c.}].$$

[Here $q = (2\pi/L)n$, with n integer.] The continuum model in Eq. (31) translates, in bosonic variables, into a quantum sine-Gordon problem[28,34]

$$\mathscr{H}_{\text{SG}} = \frac{v_S}{2}\int_0^L dx \left[K\Pi^2 + \frac{1}{K}(\nabla\Phi)^2\right] + \frac{V}{(2\pi\alpha)^2}\int_0^L dx \cos(\sqrt{16\pi}\Phi), \tag{36}$$

where we have introduced the canonical field $\Phi(x) = (\phi_+ + \phi_-)/\sqrt{4\pi}$ and its conjugate momentum $\Pi(x) = -\nabla(\phi_+ - \phi_-)/\sqrt{4\pi}$. The Luttinger model $\mathscr{H}_{\text{Luttinger}}$ is equivalent to free bosons i.e., to a massless Klein-Gordon (or Gaussian) problem ($V = 0$).[34] K is the crucial parameter governing the low-energy physics of the problem, v_S being the velocity of the sound-like gapless excitations.[34] In weak coupling we have $v_S/K = J[1 + (3J_z + J_2 + 3J_3)/\pi J + \cdots]$, and $v_S K = J[1 - (J_z - J_2 + J_3)/\pi J + \cdots]$. The umklapp term in Eq. (33), rewritten using Eq. (34), gives rise to the cosine term, with $V = -2g_3 = 2(J_z - J_2 + J_3) + \cdots$. The renormalization-group equations for the sine-Gordon problem are well known,[35,28] and have the Kosterlitz-Thouless form

$$\frac{dK}{dl} = -\tilde{V}^2(l),$$

$$\frac{d\tilde{V}}{dl} = 2[1 - 2K(l)]\tilde{V}(l), \tag{37}$$

with $\tilde{V}$ simply proportional to V. $V = 0$ with $K > 1/2$ is a line of stable fixed points which represent the Luttinger (or Gaussian) model. $V = 0$ with $K < 1/2$, on the contrary, is a line of *unstable fixed points*: the smallest $V \neq 0$ will grow upon renormalization if $K < 1/2$, the system will ''go to strong coupling'' and develop a gap in the excitation spectrum.

At the XY point, $v_S = v_F = J$ and $K = 1$. For small values of the couplings J_z, J_2, J_3 the exponent K is larger than 1/2 and the umklapp term is irrelevant, $V \to 0$. This region corresponds to a *spin liquid*. The large distance behavior of the correlation functions is characterized by power laws with exponents related to K. For instance, spin-spin correlations such as $\langle S_0^z S_n^z\rangle$ are related (recall that $S_i^z = n_i - 1/2$) to density-density correlations of the spinless fermions $\langle n(0)n(x)\rangle$. The density operator has a continuum limit expression of the type

$$n(x) \sim [\rho_+(x) + \rho_-(x)] + [\psi_+^\dagger(x)\psi_-(x) + \text{H.c.}] = \frac{1}{\sqrt{\pi}}\nabla\Phi(x) + \frac{1}{\pi\alpha}\sin[\sqrt{4\pi}\Phi(x) + 2k_F x]. \tag{38}$$

Using the fact that correlation functions of the bosonic field are simple to calculate for the Gaussian model ($V = 0$), i.e.,

$$G(x) = \langle\Phi(x)\Phi(0) - \Phi^2(0)\rangle_{V=0} = \frac{1}{4\pi}\ln\frac{\alpha^2}{\alpha^2 + x^2}, \tag{39}$$

$$\langle e^{i\gamma\Phi(x)} e^{-i\gamma\Phi(0)}\rangle_{V=0} = e^{\gamma^2 G(x)} = \left[\frac{\alpha^2}{\alpha^2 + x^2}\right]^{\gamma^2/(4\pi)}, \tag{40}$$

it is simple to show that

$$\langle n(0)n(x)\rangle = -\frac{K}{2\pi^2 x^2} + A\frac{\cos 2k_F x}{x^{2K}} + \cdots, \tag{41}$$

A being a nonuniversal constant.

Increasing the values of the couplings, the spin liquid phase becomes unstable, at $K = \frac{1}{2}$, against two different gapped phases, depending on the sign of the umklapp term V. For $V > 0$ (large values of J_z) the strong-coupling fixed point is characterized by a field Φ, which is frozen at a value such that $\cos\sqrt{16\pi}\Phi = -1$, i.e., $\sqrt{4\pi}\Phi = \pi/2$. It is then clear that density-density correlations acquire LRO, since from Eq. (38) we get

$$\langle n(0)n(x)\rangle \sim \sin(\pi/2 + 2k_F x) = \cos(2k_F x)$$

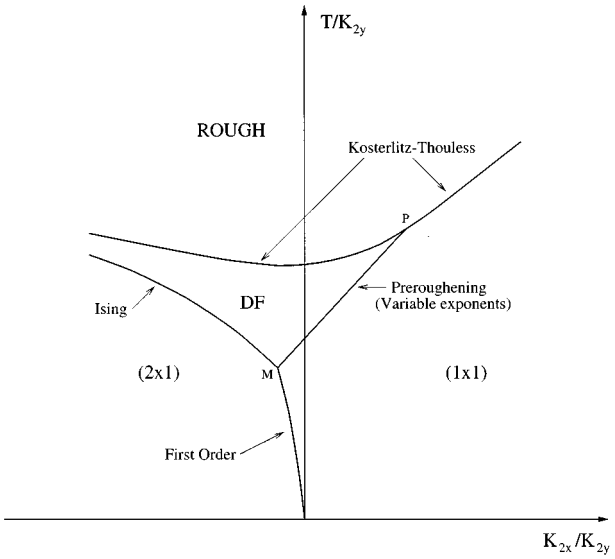

FIG. 8. Qualitative phase diagram for the modified BCSOS model in Eq. (1) for fixed values of the couplings K_3 and K_4.

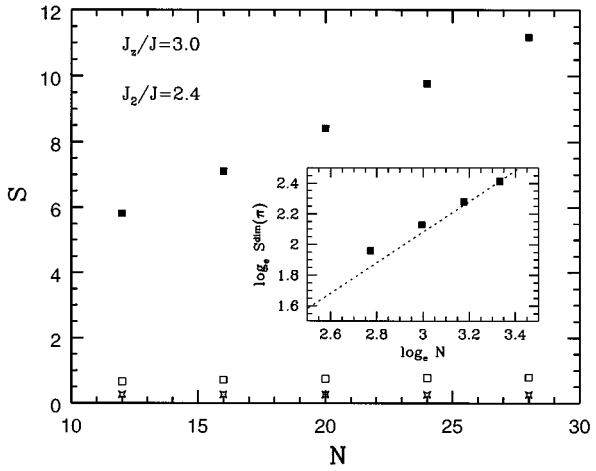

FIG. 9. Finite-size behavior of different structure factors at the point $J_z/J=3.0$ and $J_2/J=2.4$ in the dimer phase: $S^{\mathrm{dim}}(\pi)$ (solid squares), $S^{zz}(\pi)$ (crosses), and $S^{zz}(\pi/2)$ (open squares). The inset shows a logarithmic plot of the dimer structure factor, together with a dashed line of slope 1, for comparison.

signaling a site-centered $2k_F$ charge density wave. In the spin language this corresponds to a Néel phase with $\uparrow\downarrow\uparrow\downarrow$ LRO. For $V<0$, on the contrary, the strong-coupling fixed point is characterized by a field Φ, which is frozen at the value $\Phi=0$ (or 2π). To guess what correlation functions acquire LRO, notice that the canonical transformation $\psi_p\rightarrow e^{-ip\pi/4}\psi_p$ changes the sign of the umklapp term in Eq. (33), (Ref. 20) (in boson language this corresponds to $\sqrt{4\pi}\Phi\rightarrow\sqrt{4\pi}\Phi+\pi/2$). Knowing that the $2k_F$ component of the density operator acquires LRO in the Néel phase ($V>0$), we immediately conclude that the operator having LRO for $V<0$ reads

$$i[\psi_+^\dagger(x)\psi_-(x)-\mathrm{H.c.}]\sim\frac{1}{\pi\alpha}\cos[\sqrt{4\pi}\Phi(x)+2k_Fx]. \tag{42}$$

An operator whose continuum limit $2k_F$ component is given by Eq. (42) is readily found to be the bond kinetic energy $(c_i^\dagger c_{i+1}+c_{i+1}^\dagger c_i)$. The strong-coupling phase obtained for $V<0$ is therefore a *bond-centered charge-density wave*, to be contrasted to the *site-centered* CDW obtained for $V>0$. In spin language, this bond-centered CDW is a *spin dimer* phase.

Separating the Néel ($V>0$) from the dimer phase ($V<0$) is the line of unstable fixed points ($V=0$ with $K<1/2$) mentioned above. Along this line (PM in Fig. 6), the system behaves as an effective Luttinger (or Gaussian) model with $1/8<K<1/2$. If $K<1/8$, cosine terms of the type $V'\cos(2\sqrt{16\pi}\Phi)$ — formally coming from higher order umklapp processes involving four-particle scattering — become relevant and open up a gap. The nature of the transition line changes to first order. Correlation functions behave as power laws along the line PM. Density-density correlations, for instance, are still given by Eq. (41). All the critical exponents along the $V=0$ line are known in terms of K. The correlation function exponent follows directly from Eq. (41), i.e., $\eta=2K$. The gap between the ground state and the first excited state goes like[29]

$$\Delta=\frac{1}{\xi}\sim|V|^{1/(2-4K)},$$

implying a correlation-length exponent $\nu=1/(2-4K)$. The order parameter exponent is given by $\beta=\nu K$. The specific-heat exponent is $\alpha=2-2\nu=(2-8K)/(2-4K)$.

V. THE SPIN DIMER PHASE AND ITS SURFACE INTERPRETATION

In the spin dimer phase, ordinary spin-spin correlations decay exponentially to zero, but four-spin correlation functions of the type $\langle(\vec{S}_i\cdot\vec{S}_{i+1})(\vec{S}_j\cdot\vec{S}_{j+1})\rangle$ acquire LRO.[20] More specifically, everywhere inside the dimer phase in Figs. 5 and 6, one has

$$S_j^{zz}=\langle S_0^zS_j^z\rangle\rightarrow 0,\quad j\rightarrow\infty,$$

$$S_j^{\mathrm{dim}}=\langle(S_0^zS_1^z)(S_j^zS_{j+1}^z)\rangle\approx A+B(-1)^j,\quad j\rightarrow\infty. \tag{43}$$

This is illustrated in Fig. 9, where we show the size dependence of various static structure factors at the point $(J_z=3J,J_2=2.4J,J_3=0)$. These values are obtained from exact diagonalizations of chains up to 28 sites. The solid squares represent the dimer static structure factor at $q=\pi$

$$S^{\mathrm{dim}}(q=\pi)=\sum_j e^{i\pi j}S_j^{\mathrm{dim}}, \tag{44}$$

whereas the open squares and the stars represent, respectively, the $\pi/2$ and π component of the ordinary spin-spin structure factor. Clearly, $S^{\mathrm{dim}}(q=\pi)$ diverges *linearly* with the length of the chain (see inset of Fig. 9), implying long-ranged oscillations of the corresponding correlation function, whereas the usual spin-spin structure factor is finite.

To illustrate in more detail some of the physics of this disordered spin state, and its translation into the surface language, we consider a representative dimer phase point. As it happens, there is a special point in the phase diagram of the $J-J_2$ model [Eq. (22) with $J_z=J=2J_2$], where the twofold degenerate exact ground state is exactly known,[36] and extremely simple: it is just a product of spin singlets. Explicitly, for any finite (even) size N the two ground states, which turn into one another by translation of a lattice spacing, are

$$|\Psi_1\rangle=|12\rangle|34\rangle\cdots|N-1N\rangle,$$

$$|\Psi_2\rangle=|23\rangle|45\rangle\cdots|N-2N-1\rangle|N1\rangle. \tag{45}$$

Here $|ij\rangle=|\uparrow\downarrow-\downarrow\uparrow\rangle/\sqrt{2}$ denotes a singlet between sites i and j. Equation (27) is just the spinless fermion translation of Ψ_2. Some of the properties of these prototype dimer states, which we are going to illustrate, have been discussed, in connection to the DF phase problem, in Ref. 15. Obvious properties of $|\Psi_1\rangle$ are, for instance, that spin-spin correlations are extremely short ranged,

$$\langle\Psi_1|S_j^z|\Psi_1\rangle=0, \quad \forall j,$$

$$\langle\Psi_1|S_i^zS_j^z|\Psi_1\rangle=0, \quad |i-j|>1, \tag{46}$$

and that translational invariance is spontaneously broken,

$$\langle\Psi_1|S_{2j-1}^zS_{2j}^z|\Psi_1\rangle=-1/4,$$

$$\langle\Psi_1|S_{2j}^zS_{2j+1}^z|\Psi_1\rangle=0. \tag{47}$$

In spite of this order parameter, such states are clearly spin *disordered*. (1×1) order for the surface, for instance, translates into Néel LRO for the spin chain (see Fig. 3), whereas a dimer state has only short-range spin-spin correlations. To see why they describe a *flat* surface, consider expanding the product of singlets in Eq. (45) for $|\Psi_1\rangle$, say. One obtains the sum of $2^{(N/2)}$ spin configurations, one of which will be of the typical form

$$(\uparrow\downarrow)(\uparrow\downarrow)(\downarrow\uparrow)(\downarrow\uparrow)(\downarrow\uparrow)(\uparrow\downarrow)(\uparrow\downarrow)\cdots. \tag{48}$$

Here we have taken the $(\uparrow\downarrow)$ part of the singlet for the first two pairs of sites, the $(\downarrow\uparrow)$ part of the singlet for the next three pairs of sites, and so on. A *down* (2×1) step (i.e., a pair of neighboring down spins, see Fig. 2) is obtained each time a $(\downarrow\uparrow)$ pair follows immediately after a $(\uparrow\downarrow)$ one, and, vice versa, an *up* (2×1) step (a pair of neighboring up spins) results from a $(\uparrow\downarrow)$ pair following a $(\downarrow\uparrow)$ one. In between steps, there are regions with Néel type of order (unreconstructed regions in the surface language). Clearly, there is no way of having two up steps (or two down steps) following each other: a step up is followed necessarily by a step down and vice-versa. The surface is therefore *flat*.[15]

In the dimer phase there are characteristic correlations between steps that are worth stressing. An up (down) (2×1) step ending at site j is ''measured'' (see previous discussion) by the spin operator

$$\mathrm{step}_j^{\pm}=(S_{j-1}^z\pm1/2)(S_j^z\pm1/2),$$

counting, respectively, $\uparrow\uparrow$ (step^+) and $\downarrow\downarrow$ (step^-) combinations at sites $(j-1,j)$. An operator counting a step, irrespective of its being up or down, is given by

$$\mathrm{step}_j=\mathrm{step}_j^+ + \mathrm{step}_j^- = 2(S_{j-1}^zS_j^z+1/4). \tag{49}$$

One can easily work out correlation functions for such step operators in the representative dimers states. For odd j, for instance, one finds

$$\langle\Psi_1|\mathrm{step}_j^+\,\mathrm{step}_{j+n}^+|\Psi_1\rangle=\begin{cases}\frac{1}{4} & \text{if } n=0\\ \frac{1}{16} & \text{if } n>2 \text{ and even}\\ 0 & \text{otherwise,}\end{cases}$$

$$\langle\Psi_1|\mathrm{step}_j^+\,\mathrm{step}_{j+n}^-|\Psi_1\rangle=\begin{cases}\frac{1}{8} & \text{if } n=2\\ \frac{1}{16} & \text{if } n>2 \text{ and even}\\ 0 & \text{otherwise,}\end{cases}$$

$$\langle\Psi_1|\mathrm{step}_j\,\mathrm{step}_{j+n}|\Psi_1\rangle=\begin{cases}\frac{1}{2} & \text{if } n=0\\ \frac{1}{4} & \text{if } n\geqslant2 \text{ and even}\\ 0 & \text{otherwise.}\end{cases} \tag{50}$$

Similar results apply to Ψ_2 for the case of even j. It is interesting to see how closely a point inside the dimer phase of Fig. 5 resembles such an ideal scenario.[37] Figure 10 shows step-step correlations $\langle\mathrm{step}_j\mathrm{step}_{j+n}\rangle$ obtained from exact diagonalization of a chain of 28 sites, for a point inside (a) the dimer phase $(J_z=3.0J, J_2=2.4J, J_3=0)$, and (b) the Néel phase $(J_z=3.0J, J_2=J_3=0)$. In the Néel phase, $\uparrow\uparrow$ and $\downarrow\downarrow$ steps are bound in pairs, and the correlation function decays exponentially to the square of the step concentration, shown by a dashed line in Fig. 10(b). The relevant defect is therefore the domain wall denoted by $\epsilon^*_{2\times1}$ in Fig. 2. In the dimer phase, on the contrary, $\uparrow\uparrow$ and $\downarrow\downarrow$ steps are unbound, and free to move in a fluidlike manner, but their correlation function displays long-ranged oscillations with period π. In other words, the fluid of (roughly) alternating up and down steps has the feature that steps prefer to stay at an even distance from each other. In the neighboring (2×1) phase, this fluid of 2×1 steps solidifies into an ordered structure of the type $\uparrow\uparrow\downarrow\downarrow$. We stress the fact that the oscillations displayed in Fig. 10(a) are not due to (2×1) order; the point considered is, as demonstrated in Fig. 9, disordered.

Step-step correlations of the type shown are simple manifestations of the spontaneous breaking of translational invariance. Similar (and related) effects can be seen in other properties of the disordered surface. Suppose we want to count, in the surface terminology, the difference in the number of white and black local maxima in the surface. We restrict first our considerations to sites that are local maxima when considered in the x direction only. In the spin language, a local

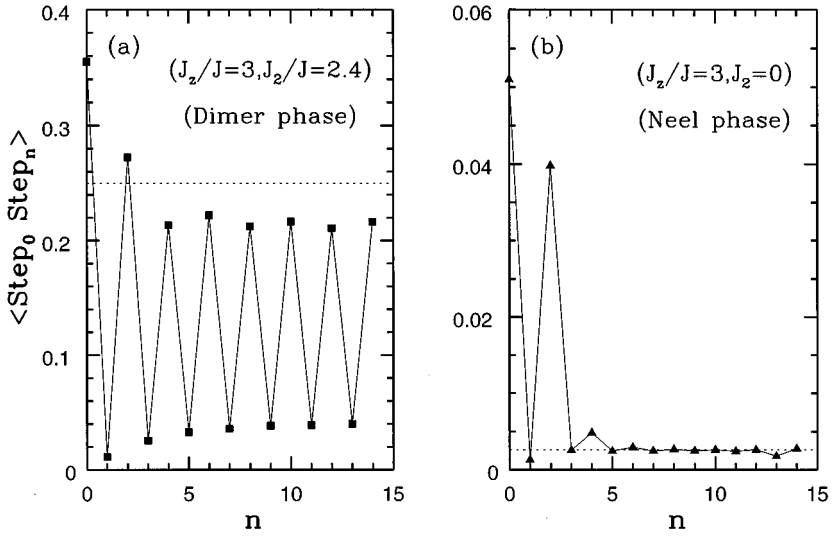

FIG. 10. (2×1) step-step correlations, see Eq. (49), for a chain of 28 sites, (a) at the point $(J_z=3.0J, J_2=2.4J, J_3=0)$ inside the dimer phase, and (b) at $(J_z=3.0J, J_2=J_3=0)$ inside the Néel phase. For the ideal dimer state Ψ_1, see Eq. (50), the correlation function would oscillate between the values 0 and 1/4 [the dashed line in (a)]. Inside the Néel phase the correlation function decays exponentially to the square of the step density, denoted by the dashed line in (b).

''maximum'' at site j occurs whenever the site $j-1$ has spin $\uparrow$ and the site j has spin $\downarrow$. An operator that ''counts'' the maximum at j is therefore $(S^z_{j-1}+1/2)(1/2-S^z_j)$. The difference between white (even j) and black (odd j) maxima is therefore measured by the order parameter

$$P^{(\mathrm{spin})}_{BW}=(2/N)\sum_j e^{i\pi j}(S^z_{j-1}+1/2)(1/2-S^z_j).$$

$P^{(\mathrm{spin})}_{BW}$ is odd under translation. Its value is 1 on the Néel state $|\uparrow\downarrow\uparrow\downarrow\cdots\rangle$, and -1 on the other Néel state $|\downarrow\uparrow\downarrow\uparrow\cdots\rangle$. Quite generally, it is different from zero in the whole Néel phase of the spin phase diagram. Consider now the value of $P^{(\mathrm{spin})}_{BW}$ on the dimer state $|\Psi_1\rangle$. Using the elementary results in Eq. (46) and (47), we arrive at

$$\langle\Psi_1|P^{(\mathrm{spin})}_{BW}|\Psi_1\rangle=-\frac{2}{N}\sum_j e^{i\pi j}\langle\Psi_1|S^z_{j-1}S^z_j|\Psi_1\rangle=\frac{1}{4}. \tag{51}$$

Similarly, $\langle\Psi_2|P^{(\mathrm{spin})}_{BW}|\Psi_2\rangle=-1/4$. Therefore, the implication of the dimer scenario, with its spontaneous breaking of translational symmetry, is that, on the disordered flat surface, one of the two sublattices tends to dominate in the local maxima.

One can check this prediction by Monte Carlo simulations of the original classical models. In the next section we will present the results of our simulations for the K_3 and the K_4 model. The results strongly support the dimer phase scenario.

VI. MONTE CARLO RESULTS AND DISCUSSION

We have performed classical Monte Carlo simulations of the K_3 and K_4 model in the DF phase. We have measured, to start with, standard quantities such as the square mean width of the surface, δh^2,

$$\delta h^2=\left\langle\frac{1}{8N_c^2}\sum_{\mathbf{r},\mathbf{r}'}(h_{\mathbf{r}}-h_{\mathbf{r}'})^2\right\rangle, \tag{52}$$

the (1×1) order parameter, $P_{1\times1}$, and the (2×1) reconstruction one, $P_{2\times1}$,

$$P_{1\times1}=\left\langle\frac{1}{N_c}\sum_{\mathbf{r}}h_{\mathbf{r}}e^{i\mathbf{G}\cdot\mathbf{r}}\right\rangle=\left\langle\frac{1}{N_c}\sum_{\mathbf{r}\in W}[h_{\mathbf{r}}-h_{\mathbf{r}+\mathbf{b}}]\right\rangle,$$

$$P_{2\times1}=\left\langle\frac{1}{2N_c}\sum_{\mathbf{r}}h_{\mathbf{r}}e^{i\mathbf{G}\cdot\mathbf{r}/2}\right\rangle. \tag{53}$$

Here N_c is the number of cells in each sublattice (i.e., $2N_c$ is the number of atoms), and $\mathbf{G}=(2\pi/a_x)\hat{\mathbf{x}}$. The square mean width δh^2 diverges logarithmically in the rough phase as the size of the sample $L\to\infty$

$$\delta h^2\approx K(T)\ln L,$$

with a coefficient $K(T)$ larger than a (universal) minimum value $K(T_R)=1/\pi^2$ attained at the roughening temperature. $P_{1\times1}$ is different from zero only in the unreconstructed region of the phase diagram and goes to zero at the preroughening line. $P_{2\times1}$ is different from zero in the reconstructed region of the phase diagram and goes to zero at the Ising line. Clearly, the DF phase has $P_{1\times1}=0$, $P_{2\times1}=0$, and $\delta h^2<\infty$. On the basis of the spin mapping and of the dimer phase scenario we expect, however, that some form of order will be present: one should be able to tell which of the two sublattices (W or B) prevails in the top layer. A way of testing this is to define the ''local peak'' operator

$$O_{\mathbf{r}}=\frac{1}{16}\prod_{i=1}^{4}[\Delta h_{\mathbf{r},i}+1], \tag{54}$$

where $\Delta h_{\mathbf{r},i}=h_{\mathbf{r}}-h_{\mathbf{r}+\mathbf{b}_i}$ and $\mathbf{b}_i$ with $i=1,\ldots,4$ are the vectors connecting a chosen site to its four nearest neighbors (belonging to the opposite sublattice). $O_{\mathbf{r}}$ takes the value 1 for the atoms lying above all their neighbors, and zero otherwise. Summing over all the sites with a phase factor 1 for the W sites and -1 for the B ones, we get a quantity measuring which sublattice prevails in the top layer,

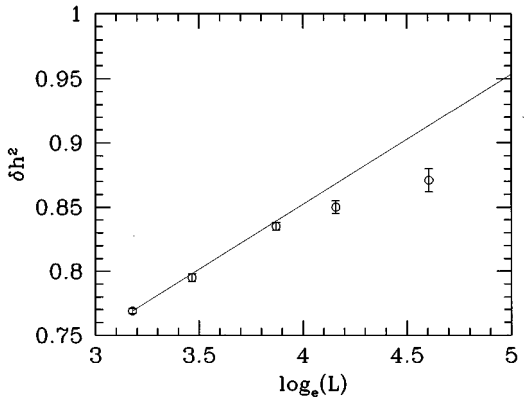

FIG. 11. Finite-size scaling of the height fluctuations, Eq. (52), for the K_3 model at $K_{2x}/K_{2y}=-0.51$, $K_3/K_{2y}=0.22$, $T/K_{2y}=3$. A line with the critical slope $K(T_R)=1/\pi^2$ is also shown, indicating that the surface is smooth at this point.

$$P_{BW}=\left\langle \frac{1}{N_c}\sum_{\mathbf{r}} e^{i\mathbf{G}\cdot\mathbf{r}}O_{\mathbf{r}}\right\rangle. \tag{55}$$

As defined, P_{BW} is normalized to 1 on the unreconstructed ground states, and to 1/2 on the reconstructed (2×1) ground states.[38] Our expectation is that *P_{BW} is different from zero in the disordered flat phase*, and vanishes in the rough region and on the *preroughening line*. (See Fig. 15.)

A classical grand-canonical single-move Monte Carlo code has been set up and used for lattices of linear size $L=N_x=N_y$ up to 100. Starting from a disordered surface, we randomly add or remove particles, making sure that the BCSOS constraint is fulfilled at each step, and accept moves according to the standard Metropolis algorithm. The configurations resulting from consecutive sweeps of the lattice ($2L^2$ attempted moves) are quite correlated, so that independent values for the various averages are obtained as a result of a sufficiently large number of Monte Carlo sweeps. It is on the basis of such ''independent measurements'' that statistical errors are estimated. Typically 20 to 50 such measurements are performed, each of which consists of 10^5-10^6 sweeps, after a suitable equilibration of the system.

For the K_3 model, we used the parameters of Mazzeo *et al.*, roughly chosen to fit the glue model results of Ercolessi, Parrinello, and Tosatti[39] for gold: $K_{2x}/K_{2y}=-0.51$, $K_3/K_{2y}=0.22$ (i.e., $\mathscr{K}=-2.3$). An Ising-type deconstruction transition has been reported to take place at $T_D\approx2.90K_{2y}$, while a Kosterlitz-Thouless roughening transition has been found at $T_R\approx3.09K_{2y}$.[11] We have performed a careful finite-size scaling analysis of the different order parameters at the intermediate temperature $T=3.0K_{2y}$.

The surface is still flat at this temperature, as demonstrated in Fig. 11, showing that δh^2 versus $\ln L$ stays definitely below the universal critical slope $K(T_R)=1/\pi^2$, which implies that δh^2 will eventually saturate to a constant as $L\to\infty$. Figure 12 (a) shows the results obtained for $P_{2\times1}$ (solid circles), and P_{BW} (diamonds). The squares denote a further order parameter used by Mazzeo *et al.*,[11]

$$P_{BW}^{(2\times1)}=\left\langle \frac{1}{4N_c}\left[\sum_{\mathbf{r}\in W}|S_{\mathbf{r}}|-\sum_{\mathbf{r}\in B}|S_{\mathbf{r}}|\right]\right\rangle, \tag{56}$$

where the classical ''spin'' variables $S_{\mathbf{r}}$ are defined in terms of the nearest-neighbor height differences as

$$S_{\mathbf{r}}=\sum_{i=1}^{4}\Delta h_{\mathbf{r},i}. \tag{57}$$

$P_{2\times1}$ vanishes as L^{-1}, see inset of Fig. 12(a), confirming that $T=3.0K_{2y}$ is above the deconstruction temperature T_D, in agreement with Ref. 11. Both P_{BW} and $P_{BW}^{(2\times1)}$ decrease, instead, much slower than L^{-1}. Figure 12 (b) shows the logarithm of P_{BW} versus $\ln L$. The data for small sizes (L up to 48) can be fit with a power law $L^{-0.37}$. For larger values of L, a crossover is seen to what is most probably an exponential convergence to *a nonzero limit* for P_{BW}. In other words, systems up to $L=48$ are still smaller than the actual value of a correlation length ξ_{BW}, so that a fictitious power-law behavior is initially seen. A similar behavior is also found for $P_{BW}^{(2\times1)}$.

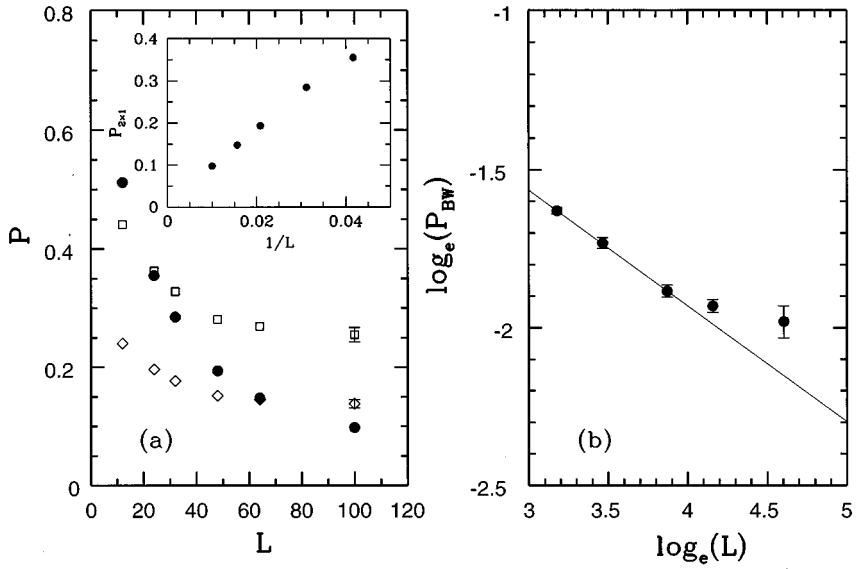

FIG. 12. (a) Finite-size scaling of $P_{2\times1}$ [the reconstruction order parameter, Eq. (53), full circles], P_{BW} [Eq. (55), open diamonds], and $P_{BW}^{(2\times1)}$ [Eq. (56, open squares] for the K_3 model at the same point considered in Fig. 11. The inset shows that $P_{2\times1}$ vanishes as the inverse of the linear size L of the lattice. The surface is thus deconstructed. (b) Log-log plot of the finite-size behavior of P_{BW}, showing the saturation to a nonzero value for $L\to\infty$. The surface is in a disordered flat state.

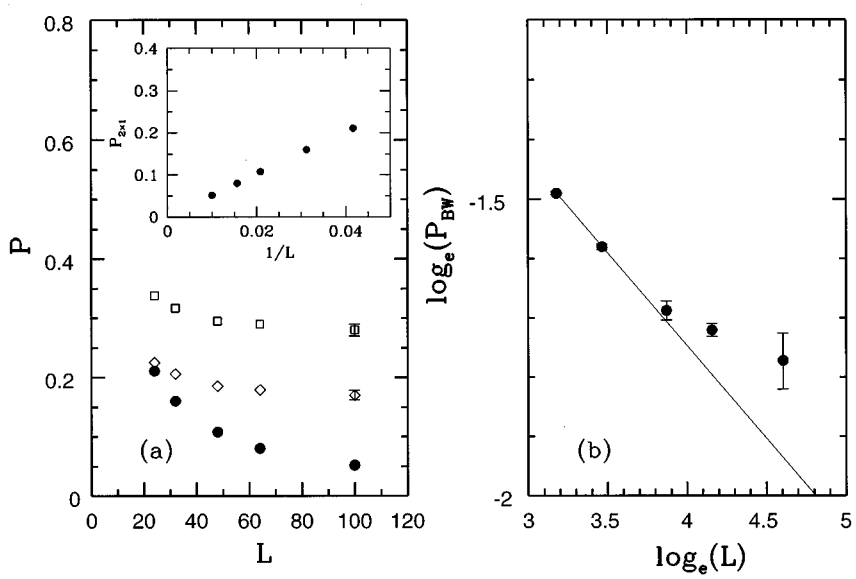

FIG. 13. Same as in Fig. 12, for a point inside the disordered flat phase of the K_4 model ($K_{2x}/K_{2y}=-0.056$, $K_4/K_{2y}=0.1$, $T/K2y=2.3$).

The corresponding results for a point inside the DF phase of the K_4 model ($K_4/K_{2y}=0.1$, $K_{2x}/K_{2y}=-0.056$, and $T/K_{2y}=2.3$) are shown in Fig. 13. Entirely similar comments apply to this case.

The point in the K_4 model phase diagram to which Fig. 13 refers, is in fact located close to the preroughening line.[18] A typical snapshot of the way this disordered flat surface looks at this temperature is shown in Fig. 14. Strictly speaking we are in a parameter region where the classical ground state is (2×1) MR reconstructed and the most energetically favored defects are *Ising* walls (see Table I). However, Ising walls in their ideal form (see Fig. 2) are almost totally absent. What one finds, instead, are extended walls of the Ising type with a width of arbitrary length. These are nothing but large (1×1) unreconstructed regions lying between two opposite (2×1) steps. Such (2×1) steps, which are the very building blocks of a MR structure, are now free to move in a fluidlike manner with the only constraint that an upstep is followed by a downstep. Occasionally, sequences of up-down (2×1) steps gain positional order by ''solidifying'' in (2×1) MR regions, which are, however, always of the same ''color'' (more precisely, black, for the phase illustrated in Fig. 14). Overall, the surface seems to have as many black regions as white ones: the $P_{1\times1}$ order parameter, which counts precisely the relative abundance of W and B (1×1) elementary cells, is small, and goes to zero in the thermodynamic limit. Correlations between steps, however, or, in more elementary terms, the fact that every (2×1) step always ends into B top atom, result in the above-mentioned feature of the absence of white MR regions, and are such that P_{BW} turns out to be different from zero, albeit small. Altogether Fig. 14 is a nice illustration of how a dimer disordered flat phase should look.

These features should be of some relevance in the context of surface scattering experiments. We discuss here the case of He scattering. In the kinematical approximation, and within a SOS framework, the intensity of the specular peak (parallel momentum transfer $\mathbf{Q}\approx0$) with perpendicular momentum transfer in the so-called antiphase configuration is given by

$$I(\mathbf{Q},q_z=\pi/a_z)\propto\left|\left\langle\sum_{\mathbf{r}}e^{i\pi h_{\mathbf{r}}}\alpha_{\mathbf{r}}\right\rangle\right|^2\delta_{\mathbf{Q},0}+N_{\text{sites}}k_BT\chi(\mathbf{Q}),\tag{58}$$

where $\alpha_{\mathbf{r}}$ is an appropriate ''shadowing factor,'' which takes into account the physical requirement that surface peaks scatter more than valleys.[40,11] The first term is a (Bragg) coherent contribution, proportional to the square of the order parameter and of the number of sites. The second contribution, due to incoherent terms, is proportional to the susceptibility of the order parameter and to the number of sites. For our BC-SOS type of model, in which $h_{\mathbf{r}}$ is even in the W sublattice, and odd in the B sublattice, one immediately concludes that $e^{i\pi h_{\mathbf{r}}}=e^{i\mathbf{G}\cdot\mathbf{r}}$ for any allowed height configuration. The coher-

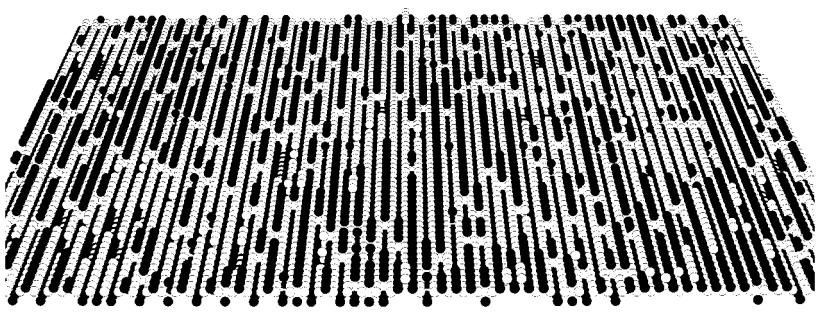

FIG. 14. Snapshot of a surface configuration as generated by the Monte Carlo simulation for the K_4 model at the same point considered in Fig. 13, inside the (dimer) disordered flat phase.

TABLE I. Ground-state energy of the defects shown in Fig. 2 for the K_3 and K_4 models.

	K_3 model	K_4 model
$\epsilon_{2\times1}$	$4K_{2x}$	$4K_{2x}+8K_4$
$\epsilon^*_{2\times1}$	$8K_{2x}$	$8K_{2x}+8K_4$
$\epsilon_{\rm CS}$	$2K_{2x}+8K_3$	$2K_{2x}+8K_4$
$\epsilon_{\rm AS}$	$-2K_{2x}$	$-2K_{2x}+8K_4$
$\epsilon_{\rm Ising}$	$-4K_{2x}$	$-4K_{2x}+8K_4$
$\epsilon^*_{\rm Ising}$	$4K_{2x}+16K_3$	$4K_{2x}+16K_4$

ent part of the specular antiphase peak $I^{\rm coh}(\mathbf{Q}=0,q_z=\pi/a_z)$ would therefore be identically zero if all the surface atoms were to scatter in the same way ($\alpha_{\mathbf{r}}=1$ for all $\mathbf{r}$). In the opposite assumption that only the local peaks scatter efficiently ($\alpha_{\mathbf{r}}=1$ if $\mathbf{r}$ is a local peak, $\alpha_{\mathbf{r}}=0$ otherwise), we obtain that $I^{\rm coh}(\mathbf{Q}=0,q_z=\pi/a_z)$ is exactly proportional to the square of the P_{BW} order parameter:[12]

$$I^{\rm coh}(\mathbf{Q}=0,q_z=\pi/a_z)\propto N^2_{\rm sites}|P_{BW}|^2. \tag{59}$$

Quite generally, for a reasonably large class of choices of shadowing factors $\alpha_{\mathbf{r}}$, the breaking of translational invariance should guarantee that $I^{\rm coh}(\mathbf{Q}=0,q_z=\pi/a_z)$ is different from zero (albeit possibly small) in the DF phase considered here. (More precisely, this is so for all the shadowing factors, which can be written in terms of local operators of the $h_{\mathbf{r}}$ variables, whose correlation function is long ranged in the DF phase.)

Experimentally, a dimer type of disordered flat phase would manifest itself with a rapid fall of the antiphase scattering as the critical temperature is approached, followed by an intermediate temperature region, where the surface is in the disordered flat phase, in which a *small coherent antiphase scattering intensity survives*. This situation is sketched in Fig. 15. By normalizing the scattering intensity to its low-temperature value, a dip at the critical temperature should be observable even if one considers the total scattering intensity $I(\mathbf{Q}=0,q_z=\pi/a_z)$, which includes the incoherent contributions. (Strictly speaking, these contributions are proportional to the susceptibility which diverges at the critical temperature as $L^{2-\eta}$, where L is the size of the system. Since $L^2=N_{\rm sites}$, the incoherent contributions will never win over the coherent part ($\propto N^2_{\rm sites}$) and an overall dip should be observable in the normalized scattering intensity at the critical temperature.) Clearly, an important requirement for the dimer scenario, which one should test experimentally, is that the dominant defects proliferating on the disordered flat surface are indeed monoatomic, or (2×1), steps. The correlations of such monoatomic steps are, at least in principle, also accessible by direct imaging techniques, such as fast STM.[41]

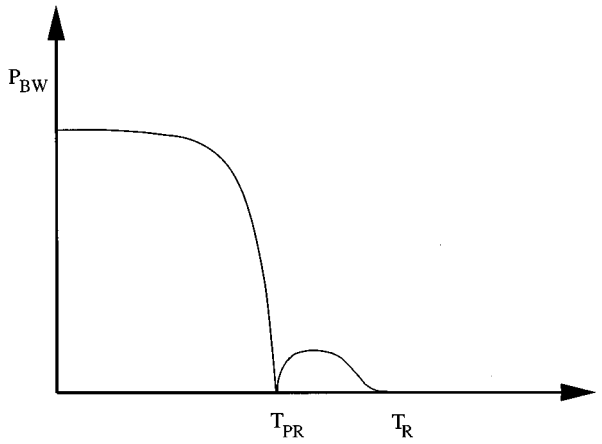

FIG. 15. Sketch of the expected behavior of the P_{BW} order parameter [Eq. (55)], proportional to the antiphase scattering intensity, as a function of temperature when the preroughening line is crossed.

We mention here, before ending the section, a particularly simple choice of shadowing factors, proposed in Ref. 40, which *does not* involve long-ranged operators:

$$\alpha_{\mathbf{r}}=2-\frac{n_{\mathbf{r}}}{2},$$

where $n_{\mathbf{r}}$ is the number of neighbors of the atom in $\mathbf{r}$ that are found at a level higher than the atom itself. This expression *linearly* interpolates between $\alpha=2$ (local maximum) and $\alpha=0$ (local minimum), and can can be recast in the form

$$\alpha_{\mathbf{r}}=1-\frac{1}{4}\sum_{i=1}^{4}[h_{\mathbf{r}+\mathbf{b}_i}-h_{\mathbf{r}}],$$

where $\mathbf{b}_i$ are the vectors connecting site $\mathbf{r}$ to the four neighboring sites. Indeed, by exploiting this linearity, it is very simple to show that such a choice of $\alpha_{\mathbf{r}}$ leads to a $I^{\rm coh}(\mathbf{Q}=0,q_z=\pi/a_z)$, which is proportional to the square of the (1×1) order parameter $P_{1\times1}$ [see Eq. (53)],

$$I^{\rm coh}(\mathbf{Q}=0,q_z=\pi/a_z)\propto\left|\left\langle\sum_{\mathbf{r}}e^{i\mathbf{G}\cdot\mathbf{r}}h_{\mathbf{r}}\right\rangle\right|^2=N_c^2|P_{1\times1}|^2, \tag{60}$$

and therefore vanishes at and beyond the preroughening line. Therefore, experimental scattering geometries should be chosen so as to emphasize peak-atom scattering, if the non monotonic behavior of Fig. 15, typical of P_{BW}, is to be detected.

VII. CONCLUSIONS

The motivation for the present work was a deeper understanding, based on well-defined Hamiltonians, of the nature of the disordered flat phase (or phases) occurring in simple lattice models of fcc (110) surfaces. In particular, for reconstructed surfaces, in the spirit of the distinction proposed in Ref. 12 between a DEF (Ising wall dominated) phase as opposed to a DOF (step dominated) phase, we wished to clarify which of the two scenarios was at play in simple BCSOS-type models. The outcome of our study is that neither of those simple prototypes applies, strictly speaking, to the description of the disordered flat phase we find, which is, on the contrary, closely related to the dimer phase of one-dimensional quantum spin-$\frac{1}{2}$ systems.

The phase diagram in Fig. 8, very similar to the one discussed in Ref. 32, shows many features that we believe to be quite robust: First, a transition between the (2×1) MR reconstructed phase and the DF phase with exponents that appear to be very close to Ising. (Although the actual nature of

the line is an open issue, see end of Sec. IV A.) Second, the transition line between the unreconstructed and the DF phase (preroughening) has variable exponents, as was predicted.[15] Third, the disordered phase has a nontrivial order parameter P_{BW}. It is quite remarkable that both the microscopic models discussed here and the cell model of Ref. 9 point in the same direction, to a disordered flat phase that has a nonvanishing order parameter of the type of P_{BW}. We recognize that such a feature is also present in the phase diagram of Ref. 32.

The obvious open question is whether the disordered phase discussed above is the only one possible. In other words, can we build microscopic models where defects other than (2×1) steps play a role and the resulting disordered flat phase (or phases) has qualitatively different features ?

The discussion has to consider separately, at this stage, the case of semimicroscopic cell-type models[9] from that of fully microscopic surface models. In the former framework of a coarse-grained description of the system, as the four-state clock-step model of den Nijs,[9] the stage is clear and the actors are there: walls and steps. Since white atoms stay on top in regions where the reconstruction variable θ is 0 or π, and black atoms do so in regions where θ is $\pi/2$ or $3\pi/2$, the P_{BW} order parameter has to be nonzero in the disordered flat phase of this model, which could therefore be called DEF. Indeed, the disordering transition resulting in a DEF phase is mostly promoted by walls, which involve a change of π for θ on either side of the defect. On the contrary, P_{BW} is expected to vanish in a hypothetical DOF phase, since in this case the relevant defects are steps, which involve a change of $\pm\pi/2$ for θ.[12] The four values of θ should appear with the same probability in such a disordered phase, and there is no way of telling which ''color'' prevails in the top atoms.

The question of possibly finding a DOF phase in the sense of Ref. 12 in a model of the clock-step type deserves, however, a few comments. Suppose that steps were indeed the most energetically favorable objects in the problem, $E_s \ll E_w$, and imagine desiring a stable DOF phase, i.e., preventing the appearance of steps from making the surface immediately rough. The natural way of doing this is to assign vertex energies to the crossing of steps, in such a way as to *disfavor the crossing of parallel steps* with respect to antiparallel ones.[15] This is indeed the standard mechanism by which a DOF is stabilized in the context of restricted SOS models for simple cubic (100) surfaces. Such six-vertex energies have been neglected by den Nijs in deriving the zero-chirality limit phase diagram for the clock-step model.[9] It is therefore an appealing suggestion, deserving further study, that their proper inclusion might open up the possibility of a genuine DOF phase in the model.[12]

Microscopic SOS models are in many ways attractive, at first sight, as far as stabilizing a DOF is concerned: they automatically tend to disfavor crossing of parallel steps that involve large height differences. Moreover, tuning the model parameters offers, in principle, the possibility of making steps *or* walls more favorable, at least as far as their $T=0$ energy is concerned. Things are, however, not so straightforward in practice. Consider, as a remarkable counterexample, the case of the K_4 model. When $-1<K_{2x}/K_4<0$, the ground state is (2×1) MR reconstructed, and simple Ising wall defects are energetically more favorable with respect to all kinds of steps (see Table I). A value of $K_{2x}/K_4=-0.56$, which we considered in one of the simulations, would have seemed therefore a quite promising candidate for a DEF phase. What we end up with instead is a situation quite well represented by the snapshot in Fig. 14. The state of the system looks as predicted for a dimer spin state. We clearly see that there are large regions in which the surface looks unreconstructed (with either the W or the B sublattice on the top layer), separated by (2×1) steps, forming a fluid with up-down order but without positional order. It is worth stressing that the relevant objects in such a disordered phase — the (2×1) steps — are the most natural defects of the *unreconstructed* surface, and the very building blocks of the neighboring MR reconstructed surface [which can be seen as a solid of alternating (2×1) steps]. The result of tailoring the $T=0$ defect energies in such a way as to promote an Ising wall dominated DEF phase ends up with an amusing realization of a dimer state instead.

In conclusion, we believe that a dimer phase type of disordered flat phase is a natural candidate in systems with a BCSOS type of symmetry such as the fcc (110) surfaces considered in this work. Experimental signatures of such a scenario would be the detection of a rapid fall of the antiphase scattering intensity as the critical temperature is approached, followed by an intermediate temperature region (before roughening) in which the dominant defects are monoatomic steps, and where a small coherent antiphase scattering intensity survives.

ACKNOWLEDGMENTS

We are grateful to Michele Fabrizio, Marco Bernasconi, Giorgio Mazzeo, Andrea Levi, and Giancarlo Jug for many instructive discussions. This research was supported by Italian Research Council (CNR) under the ''Progetto Finalizzato 'Sistemi Informatici e Calcolo Parallelo' '' and also under Contract No. 94.00708.CT02 (SUPALTEMP). We also acknowledge partial support from EEC Contract No. ERB-CHRXCT930342. G.S. acknowledges support from EEC Contract No. ERBCHBICT94.1603 during a stay at the European Synchrotron Radiation Facility (Grenoble, France) where part of the work was done.

[1] J. C. Campuzano, M. S. Foster, G. Jennings, R. F. Willis, and W. Unertl, Phys. Rev. Lett. **54**, 2684 (1985); J. Sprösser, B. Salanon, and J. Lapujoulade, Europhys. Lett. **16**, 283 (1991); D. Cvetko, A. Lausi, A. Morgante, F. Tommasini, and K. C. Prince, Surf. Sci. **269/270**, 68 (1991), and references therein.

[2] I. K. Robinson, E. Vlieg, and K. Kern, Phys. Rev. Lett. **63**, 2578 (1989); M. Kryzowski and K. Kern (private communication).

[3] K. Kern, in *Phase Transitions in Surface Films 2*, Vol. 267 of *NATO Advanced Studies Institute, Series B: Physics*, edited by H. Taub *et al.* (Plenum Press, New York, 1990), p. 269, and references therein.

[4] Y. Cao and E. H. Conrad, Phys. Rev. Lett. **64**, 447 (1990).

[5] M. Garofalo, E. Tosatti, and F. Ercolessi, Surf. Sci. **188**, 321 (1987); A. Trayanov, A. C. Levi, and E. Tosatti, Europhys. Lett. **8**, 657 (1989).
[6] J. Villain and I. Vilfan, Surf. Sci. **199**, 165 (1988).
[7] J. Kohanoff, G. Jug, and E. Tosatti, J. Phys. A **23**, L209 (1990); **23**, 5625 (1990).
[8] I. Vilfan and J. Villain, Surf. Sci. **257**, 368 (1991).
[9] M. den Nijs, Phys. Rev. B **46**, 10 386 (1992).
[10] L. Balents and M. Kardar, Phys. Rev. B **46**, 16 031 (1992).
[11] G. Mazzeo, G. Jug, A. C. Levi, and E. Tosatti, Surf. Sci. **273**, 237 (1992); Europhys. Lett. **22**, 39 (1993).
[12] For a review, see M. Bernasconi and E. Tosatti, Surf. Sci. Rep. **17**, 363 (1993).
[13] M. den Nijs, Phys. Rev. Lett. **64**, 435 (1990).
[14] G. Jug and E. Tosatti, Phys. Rev. B **42**, 969 (1990).
[15] M. den Nijs and K. Rommelse, Phys. Rev. B **40**, 4709 (1989).
[16] Balents and Kardar (Ref. 10) have independently analyzed the fermionic problem obtaining a completely similar phase diagram.
[17] H. van Beijeren, Phys. Rev. Lett. **38**, 993 (1977).
[18] G. Santoro and M. Fabrizio, Phys. Rev. B **49**, 13 886 (1994).
[19] A beautiful discussion of the physics of 1D quantum spin systems and the connections to the disordered flat phase of SOS models is given by den Nijs and Rommelse in Ref. 15. Relevant studies on quantum-spin chains are also: T. Kennedy and H. Tasaki, Commun. Math. Phys. **147**, 431 (1992); K. Hida, Phys. Rev. B **45**, 2207 (1992).
[20] F. D. M. Haldane, Phys. Rev. B **25**, 4925 (1982); **26** 5257 (E) (1982).
[21] J. D. Weeks, in *Ordering in Strongly Fluctuating Condensed Matter System*, Vol. 50 of *NATO Advanced Studies Institute Series B: Physics*, edited by T. Riste (Plenum, New York, 1979).
[22] J. Kohanoff and E. Tosatti (unpublished).
[23] The qualitative difference between Figs. 7 and 8 is related to the pathological behavior of the K_3-model for $K_{2x}\to 0$.
[24] J. B. Kogut, Rev. Mod. Phys. **51**, 659 (1979).
[25] M. den Nijs, in *Phase Transitions and Critical Phenomena*, edited by C. Domb and J. L. Lebowitz (Academic, London, 1988), Vol. 12, p. 219.
[26] For given values of the classical couplings, increasing the temperature from $T=0$ to $T=\infty$ amounts to moving the representative point in the quantum phase diagram along a straight line, starting from large values of J_z/J, J_2/J, J_3/J, and going towards the point $J_z=J_2=J_3=0$.
[27] The sign of the spin-flip term in Eq. (21) can be changed by the canonical transformation $S_i^{\pm}\to(-1)^i S_i^{\pm}$. A singlet pair has the standard sign, $(\uparrow\downarrow-\downarrow\uparrow)$, in the new representation, whereas it reads $(\uparrow\downarrow+\downarrow\uparrow)$ in the representation in which the spin-flip term has a negative matrix element.
[28] K. Nomura and K. Okamoto, J. Phys. A **27**, 5773 (1994).
[29] J. Sólyom, Adv. Phys. **28**, 201 (1979).
[30] H. J. Schulz and T. Ziman, Phys. Rev. B **33**, 6545 (1986).
[31] The difference is essentially due to the fact that our second-neighbor coupling in Eq. (21) is of the Ising type ($J_2 S_i^z S_{i+2}^z$) as opposed to being spin isotropic as it is in the $J-J_2$ model. For large values of J_2 the model in Eq. (2) with $J_3=0$ maps onto two uncoupled antiferromagnetic Ising chains. Given the large gap of the Ising problem, a small nearest-neighbor XXZ term has no effect on it and the systems remains ordered. On the contrary, the spin-isotropic model in Eq. (22) maps, for large J_2, onto two uncoupled isotropic Heisenberg chains, which are gapless and for which the nearest-neighbor XXZ term is a relevant perturbation.
[32] P. J. M. Bastiaansen and H. J. F. Knops, Phys. Rev. B **53**, 126 (1996).
[33] G. Mazzeo, E. Carlon, and H. van Beijeren, Phys. Rev. Lett. **74**, 1391 (1995).
[34] F. D. M. Haldane, J. Phys. C **14**, 2585 (1981).
[35] The renormalization is performed by scaling the cutoff $\alpha\to e^l\alpha$ with $l>0$. See, for instance, T. Giamarchi and H. J. Schulz, J. Phys. (Paris) **49**, 819 (1988).
[36] C. K. Madjumdar and D. K. Ghosh, J. Phys. C **3**, 911 (1970). For a quite detailed and elementary account of models having simple ground states of this type see, for instance, W. J. Caspers, *Spin Systems* (World Scientific, Singapore, 1989).
[37] It is worth mentioning here what happens to (3×1) steps, i.e., three neighboring like-spins ($\uparrow\uparrow\uparrow$ for up steps and $\downarrow\downarrow\downarrow$ for down steps). Such objects — strictly absent in the two representative dimer states in Eq. (45) — are quite rare in the dimer phase and play no role: their correlation function decays exponentially to the square of their concentration without any form of LRO.
[38] P_{BW} coincides, apart from a factor 2, with the order parameter P_{EO} defined in Ref. 12. To avoid possible misunderstandings, we mention that in Ref. 11 P_{BW} denotes the order parameter of the unreconstructed surface $P_{(1\times 1)}$.
[39] F. Ercolessi, M. Parrinello, and E. Tosatti, Philos. Mag. A **58**, 213 (1988).
[40] A. C. Levi, R. Spadacini, and G. E. Tommei, in *The Structure of Surface II*, edited by J. F. van der Veen and A. Hove (Springer-Verlag, Berlin, 1988), Vol. 11.
[41] L. Kuipers, M. S. Hoogeman, and J. W. M. Frenken, Phys. Rev. Lett. **71**, 3517 (1993).